NANOSTRUCTURED AND POROUS HIGH TEMPERATURE CERAMICS USING BLOCK COPOLYMER MESOPHASES

A Dissertation

Presented to the Faculty of the Graduate School

of Cornell University

In Partial Fulfillment of the Requirements for the Degree of

Doctor of Philosophy

by

Maria Magdalena Gerdina Kamperman

August 2008

NANOSTRUCTURED AND POROUS HIGH TEMPERATURE CERAMICS USING BLOCK COPOLYMER MESOPHASES

Maria Magdalena Gerdina Kamperman, Ph. D.

Cornell University 2008

Nanostructured high-temperature ceramics offer great promise in various applications, because of their excellent thermal stability and mechanical properties. Despite advances in oxide materials, nanostructuring of high temperature non-oxide ceramics such as silicon carbonitrides (SiCN) or silicon carbides (SiC) has remained a major challenge. This dissertation describes a well controlled bottom-up approach to overcome this challenge. Block copolymer mesophases are used to structure direct polymer derived ceramic (PDC) precursors on the nanoscopic scale. Subsequent high temperature treatment enables, for the first time, the preparation of mesoporous ceramic materials stable up to 1500 ºC.

By blending with an amphiphilic block copolymer, the PDC precursor is expected to selectively swell the hydrophilic block of the polymer. The hybrid morphology can be controlled by systematically increasing the PDC precursor/ block copolymer ratio or by changing characteristics, like the molecular weight of the block copolymer. In fundamental studies to establish hybrid composition structure correlations it is demonstrated that PUMVS is susceptible to reaction with water leading to replacement of nitrogen by oxygen, which can be circumvented by working under dry conditions.

Finally, we combine this block copolymer based approach with micromolding and multi-component colloidal self-assembly to make three-dimensionally interconnected, high temperature ceramic materials structured on eight distinct length

scales and integrating catalytic functionality from well-dispersed platinum nanoparticles.

BIOGRAPHICAL SKETCH

Marleen was born and raised in IJsselstein, the Netherlands. She moved to the north of the country to study chemistry, with a major in polymer chemistry, at the University of Groningen. The research she performed in the groups of Prof. A.J. Schouten and Prof. J.A. Wesselingh on reactive hot-melt adhesives for car windows was performed as a partnership between the university and the industrial company ICI. She received a M.S. degree in Chemistry in 2003. She continued her studies at Cornell University where she joined the Wiesner group in the Materials Science & Engineering department and worked on the development of ordered mesoporous high temperature ceramics using block copolymers. After finishing her Ph.D. she will join the group of Prof. Eduard Arzt at the Institute of New Materials in Saarbrücken, Germany, as a postdoctoral researcher.

ACKNOWLEDGEMENTS

This work would not have been possible without the help of a great number of people. First, I would like to thank my advisor Prof. Uli Wiesner. His enthusiasm and creativity were a great motivation and inspiration. I also would like to thank my other committee members Prof. Frank DiSalvo and Prof. Chekesha Liddell for their support, Prof. Lara Estroff for being a great role model and Prof. Sol Gruner for placing enough trust in me to let me use his X-ray scattering equipment.

Many thanks to the Wiesner group; I had a wonderful time with you and I have never worked with such a diverse group of people. Thanks to the talented and great undergraduate students that I worked with; Raluca Scarlat, Billy Yau, Melissa Fierke, Robert Weissgraeber, Brian Goodfellow and Kelly Johansen.

I received a considerable amount of help and guidance from several people outside of the Wiesner group. Thanks to Gil Toombes and Mark Tate for their invaluable help with the X-ray scattering experiments, Shahyaan Desai for all his help in the clean room, Arthur Woll for his help at CHESS and Prof. Josef Zwanziger, Ulrike Zwanziger, Prof. H.W. Spiess and Robert Graf for their Solid State NMR expertise.

Having access to the facilities at Cornell University has been a real privilege. My thanks to the facility managers of Cornell Center of Materials Research for all their help and training: Paul, John S., Yuanming, John G., John H., Maura and Tony.

Thanks to the always friendly people in the Bard Hall office: Patty, Vicki, Carol, Joseph, Dolores, Verne, Michele and Laura. Thank you Sara Hernandez and DiOnetta Jones for showing me how to combine femininity and professionalism.

Special thanks to Stephanie for being such a great friend, for all your advice from how to write cover letters to getting good deals on plane tickets and for being

such a great listener. Thanks to Baski and Poorna for the friendship and all the coffee and Scotch: you are awesome. Monique, thank you for your friendship and for preparing me for my post-doc experience by being a post-doc yourself. Gerlof for all the postcards and for making me the unofficial witness of your wedding. The Dutch boys Guus, Micha, Niels, Willem, JP and Kuik for the good old times. To my parents, Renske, Hans en Geert for being the best family in the world. Owen, thank you for giving ‘dat stukje jeu aan mijn leven’.

TABLE OF CONTENTS

LIST OF FIGURES

LIST OF TABLES

CHAPTER 1

INTRODUCTION

One of the fundamental structure directing processes in nature is provided by self-assembly of amphiphilic molecules. The universality of pattern formation by liquid crystals, lipid membranes, and block copolymers [1–3], all soft materials that are closely related to biological motifs, is striking. The resulting soft structures are often due to a balance of forces minimizing the Gibbs free energy and are at dynamic equilibrium [4]. In the case of block copolymers, important contributions to the free energy are the configurational entropy of the molecules and the formation of interfacial area. The theory, which describes these phenomena, is well developed [5] and gives reasonable predictions of phase behavior. In the meantime, this knowledge about block copolymer phase behavior has been utilized to structure direct other organic as well as inorganic materials for formation of composite and porous structures [6-10]. The most common route for preparing organic-inorganic hybrid materials is by using sol-gel chemistry. A solution containing inorganic precursors and block copolymer can be used to co-assemble different mesophases. Significant research efforts were devoted on amphiphilic macromolecules and inorganic precursors demonstrating the versatility of this approach. The majority of these studies were focused on metal oxide systems [8].

It is an interesting challenge to move away from oxide structures and generalize the block copolymer approach towards high temperature non-oxide type ceramics. Materials such as SiN_xC_y have been heavily investigated in their own right because of their high thermal stability and mechanical properties [11, 12]. Among a variety of methods to produce SiCN-type ceramics the use of polymer derived ceramics (PDCs) is particularly interesting. PDCs can be processed at temperatures

lower than those required in conventional fabrication methods and can be shaped into complex structures. Subsequent heat treatment transforms the polymeric precursors into ceramic materials, while retaining the original shape. These materials are used in a variety of applications ranging from microelectronic mechanical systems (MEMS), coatings and fibers [13-15]. More recently PDC precursors were employed for the synthesis of macroporous SiC and SiN_xC_y materials, by mixing with polystyrene or silica templates [16, 17].

In this dissertation, I report on the development of a bottom-up approach in which block copolymers are used to structure direct PDC precursors. Chapter 2 describes with the concept of blending the amphiphilic block copolymer, poly(isoprene-*block*-dimethylamino ethylmethacrylate) (PI-*b*-PDMAEMA) with poly(ureamethylvinyl) silazane (PUMVS). PUMVS selectively swelled to the hydrophilic block. The structure of the resulting composites was set by crosslinking the PUMVS. Heat treatment converted the composites into ordered mesoporous ceramic materials stable up to 1500 ºC.

Chapter 3 gives a detailed description of the synthesis and structural characterization of materials from their as-made state all the way to the ordered porous ceramic materials. Rutherford Back Scattering (RBS) and solid state NMR experiments showed that to control the chemical composition of the hybrid materials the PUMVS, which reacts with water, must be kept away from all sources of moisture. Various morphologies with variable lattice spacings were accessible for composites with PUMVS including hexagonal and lamellar morphologies, as was verified by small angle X-ray scattering (SAXS) and transmission electron microscopy (TEM). In addition to the preparation of bulk materials, dissolution of hexagonal/lamellar hybrids rich in PI led to nanoparticles of well defined shape and size.

In Chapter 4, the effect of using a semicrystalline (PI-*b*-PEO) versus an amorphous block copolymer (PI-*b*-PDMAEMA) as structure directing agent for PUMVS, on hybrid morphology is investigated. It is shown that in the case of PI-*b*-PEO upon crystallization of the PEO, a crystalline lamellar morphology is obtained for most PUMVS/ block copolymer ratios. The overall periodicity of the PI-*b*-PEO/ PUMVS hybrids increased only slightly upon increased PUMVS loading, because the strong chain stretching in the PI block is progressively relaxed as the PUMVS swells the PEO. Suppression of crystallization through high temperature annealing results in morphological behavior that is expected from typical block copolymer phase diagrams and is similar to the amorphous PI-*b*-PDMAEMA/PUMVS system.

In the last chapter a method is presented to produce porous high temperature ceramics with functionality integrated from the atomic to macroscopic level. These materials are promising especially for size-selective catalysis and microreactor applications. The challenge was to achieve the following properties *within the same material*: 1) high surface area per unit volume to reduce the required catalyst volume for a given conversion; 2) stability at high temperatures, ideally 800°C or higher, to avoid coking of the catalyst; and 3) an acceptable pressure drop. Through a combination of characterization techniques including scattering (SAXS/WAXS) and imaging (TEM/SEM), it was shown that the developed materials satisfy all three key requirements. The macroscopic structuring was obtained by a combination of micromolding and multi-component colloidal self-assembly. The resulting template was filled with a five component solution containing solvent, block copolymer, ceramic precursos with a radical initiator and nanoparticle catalyst. Heating the resulting material to 1000°C resulted in a three-dimensional, interconnected, porous, high temperature stable ceramic material structured over eight discrete length scales and functionalized with well-dispersed 1-2 nm platinum catalyst nanoparticles.

The presented block copolymer directed co-assembly (bottom-up) approach, described in this thesis, thus provides a versatile method to synthesize structured high temperature non-oxide-type ceramics from PDCs with tunable morphology, domain size, composition and functionality.

REFERENCES

[1] P. Ball, *The Self-Made Tapestry,* Oxford University Press, Oxford, **1998**.

[2] J. M. Seddon, *Biochim. Biophys. Acta* **1990**, 1031, 1.

[3] I. W. Hamley, *The Physics of Block Copolymers,* Oxford University Press, Oxford, **1998**.

[4] V. Luzzati, T. Gulik-Krzywicki, A. Tardieu, *Nature* **1968**, *218,* 1031.

[5] M. W. Matsen; F. S. Bates, *Macromolecules* **1996**, *29*, 1091.

[6] M. Templin, A. Franck, A. Du Chesne, H. Leist, Y. M. Zhang, R. Ulrich, V. Schädler, U. Wiesner, *Science* **1997**, *278*, 1795.

[7] D. Zhao, J. Feng, Q. Huo, N. Melosh, G. H. Fredrickson, B. F. Chmelka, G. D. Stucky, *Science* **1998**, *279*, 548.

[8] M. Kamperman, U. Wiesner, in *Block Copolymers in Nanoscience* (Eds.: M. Lazzari, G. Liu, S. Lecommandoux), Wiley-VCH, Weinheim, **2006**.

[9] M. A. Hillmyer, P. M. Lipic, D. A. Hajduk, K. Almdal, F. S. Bates, *Journal of the American Chemical Society* **1997**, *119*, 2749.

[10] C. B. W. Garcia, C. Lovell, C. Curry, M. Faught, Y. M. Zhang, U. Wiesner, *J. Polym. Sci. B: Polym. Phys.* **2003**, *41*, 3346-3350.

[11] Y. L. Li, E. Kroke, R. Riedel, C. Fasel, C. Gervais, F. Babonneau, *Applied Organometallic Chemistry* **2001**, *15*, 820.

[12] S. R. Shah, R. Raj, *Acta Materialia* **2002**, *50*, 4093.

[13] R. Raj, R. Riedel, G. D. Soraru, *Journal of the American Ceramic Society* **2001**, *84*, 2158.

[14] D. Seyferth, C. Strohmann, N. R. Dando, A. J. Perrotta, *Chemistry of Materials* **1995**, *7*, 2058.

[15] J. M. Schwark, *Polymer Preprints* **1991**, *32*, 567.

[16] Y. F. Shi, Y. Meng, D. H. Chen, S. J. Cheng, P. Chen, H. F. Yang, D. Y. Zhao, *Advanced Functional Materials* **2006**, *16*, 561.

[17] I. K. Sung, Christian, M. Mitchell, D. P. Kim, P. J. A. Kenis, *Advanced Functional Materials* **2005**, *15*, 1336.

CHAPTER 2

ORDERED MESOPOROUS CERAMICS STABLE UP TO 1500 °C FROM DIBLOCK COPOLYMER MESOPHASES[1]

Abstract

In the present study a poly(isoprene-*block*-dimethylamino ethylmethacrylate), diblock copolymer (PI-*b*-PDMAEMA) is used to structure direct a polysilazane pre-ceramic polymer, commercially known as Ceraset. To the polymer a two-fold excess in weight of the silazane oligomer (Ceraset) was added. The resulting composite was cast into films and after cooperative self-assembly of block copolymer and Ceraset, the structure was permanently set in the hexagonal columnar morphology as evidenced by small angle X-ray scattering (SAXS) and transmission electron microscopy (TEM). Crosslinking of the silazane oligomer was achieved with a radical initiator at 120°C. Upon heating the composite to 1500°C under nitrogen the structure is preserved and a mesoporous ceramic material is obtained, as demonstrated by SAXS and TEM. The pores are open and accessible as evidenced by nitrogen sorption/desorption measurements indicating a surface area of about 41 m^2g^{-1} and a pore diameter of 13 nm, consistent with TEM analysis. These results suggest that the use of block copolymer mesophases may provide a simple, easily controlled pathway for the preparation of various high temperature ceramic mesostructures.

---

[1] Reproduced with permission from: Kamperman, M.; Garcia, C. B. W.; Du, P.; Ow, H. S.; Wiesner, U. *Journal of the American Chemical Society* **2004**, *126*, 14708-14709. Copyright 2004 American Chemical Society.

The synthesis of mesoporous silica-type ceramic materials through co-assembly of silica sources with organic structuredirecting agents has been the focus of intense research activities over the past decade. The field was pioneered by a seminal research paper from scientists of the Mobil Corp. in 1992 about lowmolecular-weight ionic surfactant-templated synthetic procedures [1]. In the second half of the 1990s, macromolecular nonionic surfactants were used for the first time to structure-direct orthosilicates [2,3] and organically modified silica precursors [4] from aqueous solutions and organic solvents, respectively, extending the accessible pore sizes of the resulting mesoporous materials to hundreds of angstroms. Shortly afterward, this approach was generalized to other metal oxides [5]. Despite these advances, nanostructuring of high temperature non-oxide ceramics such as silicon carbonitrides (SiCN) or silicon carbides (SiC) has remained a major challenge. In 2003, we reported an amphiphilic poly(isoprene-*block*-ethylene oxide) diblock copolymer (PI-*b*-PEO) as a structure-directing agent for a polysilazane pre-ceramic polymer commercially known as Ceraset [6]. This work paved the way toward the preparation of various high temperature SiCN-type ceramic mesostructures [7]. Further unpublished studies in our laboratories showed, however, that this approach failed to produce porous high-temperature ceramics. In the present contribution we show the preparation of mesoporous ceramic materials stable up to 1500 °C based on a related approach using poly(isoprene-*block*-dimethylamino ethyl methacrylate) (PI-*b*-PDMAEMA) as the structure-directing agent for Ceraset (see Figure 2.1). Deviation from PEO as the hydrophilic block is motivated by limited PEO/Ceraset miscibility and PEO crystallization in polymer/Ceraset composites (both PI and PDMAEMA are amorphous polymers).

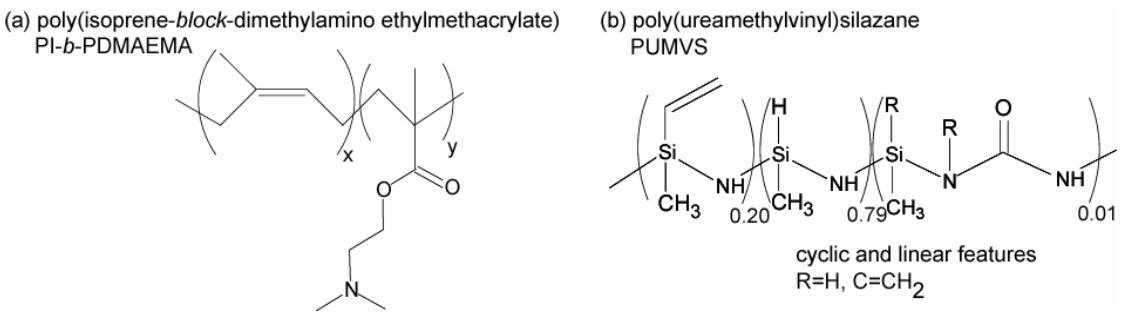

Figure 2.1. Chemical structures of (a) poly(isoprene-*block*-dimethylamino ethyl methacrylate) and (b) Ceraset, a polyureamethylvinylsilazane.

The block copolymer PI-*b*-PDMAEMA was synthesized using anionic polymerization as described elsewhere [8]. The physical characteristics of the polymer **MK1** studied here were determined by gel-permeation chromatography (GPC) and ^{1}H NMR. The resulting polymer had a molecular weight of 20 100 g/mol and 26 wt % PDMAEMA with polydispersity index below 1.2. Ceraset (KiON Corp.) and the radical initiator, dicumyl peroxide (Aldrich), were used as received. The chemical structures of block copolymer and Ceraset are shown in Figure 2.1. In a typical synthesis, a 5 wt % block copolymer solution in tetrahydrofuran (THF) was mixed with the radical initiator (1-0.5 wt % with respect to the mass of Ceraset added) and the silazane precursor and stirred for 1 h. The solution was poured into a Petri dish and a film cast by solvent evaporation on a hot plate at 50 °C for 3 h. The film was then annealed in a vacuum oven for 24 h at 50 °C and subsequently ramped up to 120 °C for 1 h to cross-link the silazane. Here we will discuss a composite **MK1/1** with a polymer-to-Ceraset weight ratio of 1/2. After structure analysis, the composite was heat-treated using 1 °C/min ramps under nitrogen up to temperatures as high as 1500 °C for conversion into the high-temperature ceramic material.

Blending the silazane with the block copolymer is expected to lead to preferential segregation of the silazane within the PDMAEMA domains, primarily due to the polar nature of the molecule (see Figure 2.1). This increases the effective

volume fraction of the PDMAEMA domains. By taking a block copolymer of a given composition, different morphologies should thus be accessible by simply increasing the amount of the silazane oligomer added, similar to what was observed in systems described earlier [6,9,10]. Polymerization of the silazane is then started through the thermally activated radical initiator, dicumyl peroxide, within the PDMAEMA/Ceraset domains. This generates a nanostructured composite consisting of PI and PDMAEMA/cross-linked polysilazane mixed domains.

Small-angle X-ray scattering (SAXS) experiments were performed on a Bruker-AXS Nanostar (Cu KR, 1.54 Å) operated at 40 kV, 40 mA in transmission mode. In the SAXS pattern of composite **MK1/1** after cross-linking at 120 °C (Figure 2.2a), peaks with *q* spacing ratios of 1, $\sqrt{3}$, $\sqrt{4}$ and $\sqrt{7}$ are discernible, consistent with hexagonally packed domains.

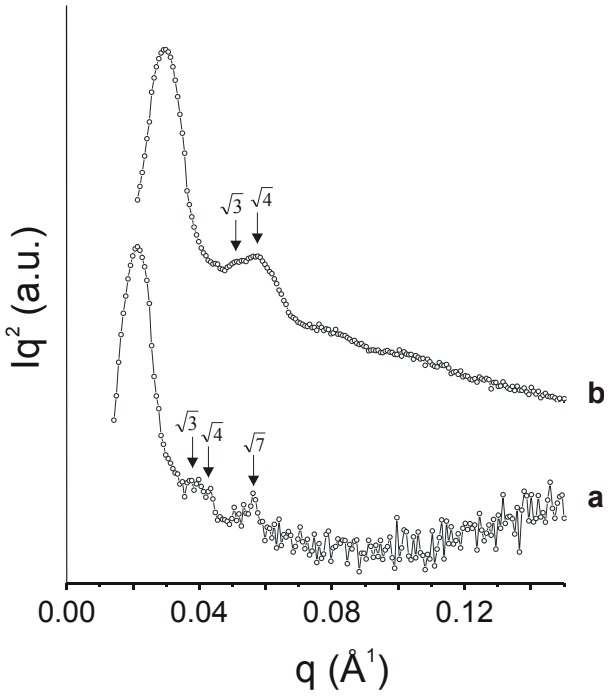

Figure 2.2. SAXS traces of the as-made composite (a) and ceramic after calcination to 1500 °C (b). Peak positions as expected for a hexagonal cylinder morphology are indicated by tics.

Transmission electron microscopy (TEM) was performed on a JEOL 1200EX operating at 120 keV to corroborate this assignment. Bulk samples were embedded in epoxy and 50-100 nm sections cut using a Leica Ultracut UCT microtome at -60 °C for composites and at room temperature for ceramics. Sections were subsequently transferred to copper grids for analysis. A representative TEM image of the composite is shown in Figure 2.3a. The contrast in this micrograph arises from the electron density difference between PI and PDMAEMA/ polysilazane domains, the latter appearing darker. The image of **MK1/1** clearly shows hexagonally packed cylinders.

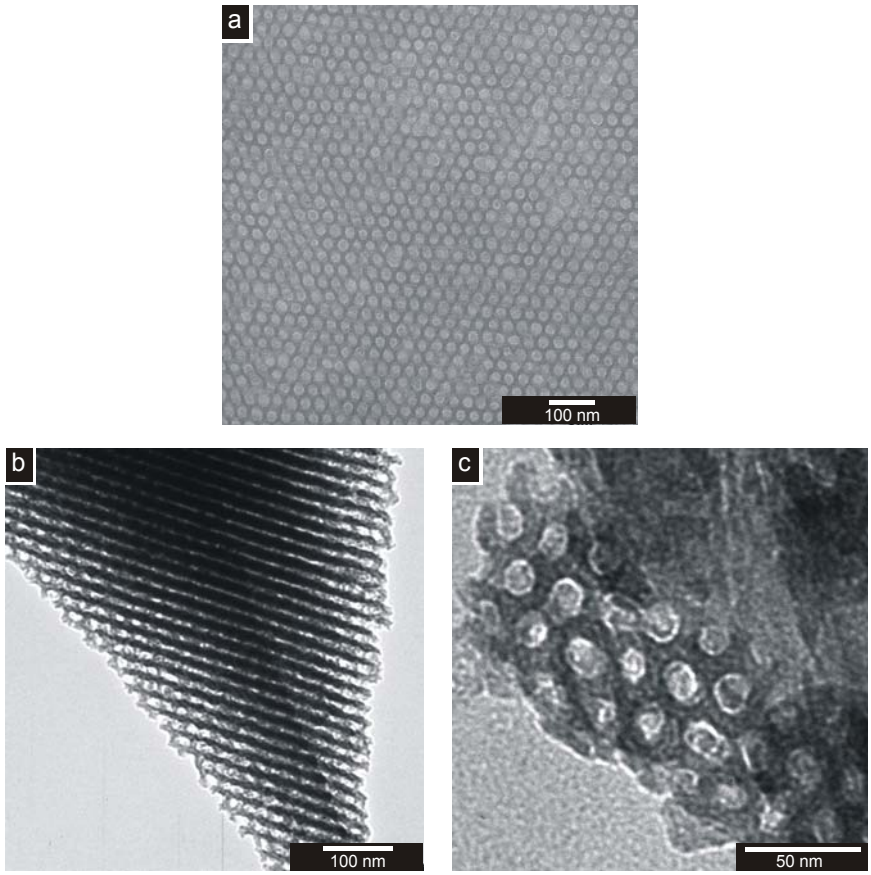

Figure 2.3. Bright-field TEM images of the as-made composite (a) and ceramic calcined to 1500 °C (b), demonstrating that the hexagonal structure is preserved during heat treatment.

The SAXS diffractogram of sample **MK1/1** after heat treatment to 1500 °C is shown in Figure 2.2b. Although for both traces (a) and (b) the measuring time was about 1 h, the signal-to-noise ratio is clearly better for trace (b), expected from a higher electron density contrast in this sample. Besides the first-order peak, two higher order reflections at q spacing ratios of $\sqrt{3}$ and $\sqrt{4}$ of the firstorder maximum are clearly visible for the ceramic, consistent with preservation of a hexagonal structure. There is a significant shift of the spectrum to higher q-values compared to the composite, indicating sample shrinkage upon high-temperature treatment. The (10) plane spacing is found to decrease from 31 to 22 nm on going from the composite to the ceramic material. That the hexagonal structure is preserved upon heating to 1500°C is corroborated by the TEM images in Figure 2.3b and c, which show different projections of hexagonally packed cylinders. From Figure 2.3c, the average pore diameter can be estimated as ~13 nm.

From the SAXS and TEM results, heat treatment up to 1500 °C of the bulk composite preserves the nanostructure and leads to a mesoporous material. Separate microprobe studies (JEOL 8900 EPMA) of the composition of these materials treated up to 1400- 1500 °C under Ar/H2 typically showed the following number percentages: 29% C, 9% O, 30% N, and 32% Si. To check whether the pores are open and accessible, nitrogen adsorption-desorption isotherms were measured on a Micromeritics ASAP 2020 at 77 K after outgassing at 100 mPa for 15 h at 300 °C. In Figure 2.4, the porous ceramic exhibits a nitrogen sorption isotherm of type IV according to BDDT classification, with a specific surface area of 51 $m^2 g^{-1}$ according to the Brunnauer-Emmett-Teller (BET) method [11]. Calculation of the pore size distribution from the adsorption branch of the isotherm reveals an average pore diameter according to Barrett-Joyner-Halenda [12] (BJH) of 13 nm, which is in excellent agreement with the TEM results. The measured surface area per gram of the

mesoporous ceramic is considerably lower than what is typically observed in block copolymer-directed mesoporous silica, where both meso- and micropores are present [3,9]. The contribution from the mesopores to surface area in the present material can be estimated from the structural information obtained from SAXS and TEM. The calculation is based on the pore diameter of 13 nm, determined from TEM (consistent with results of the nitrogen sorption/desorption experiments), the (10) plane spacing of the hexagonally packed cylindrical pores from SAXS (22 nm), and an approximate density of 2.5 g/cm^3 [13]. The resulting surface area of 38.2 m^2 g^{-1} is in good agreement with the value obtained from the BET analysis and suggests that wall microporosity contributions are probably small.

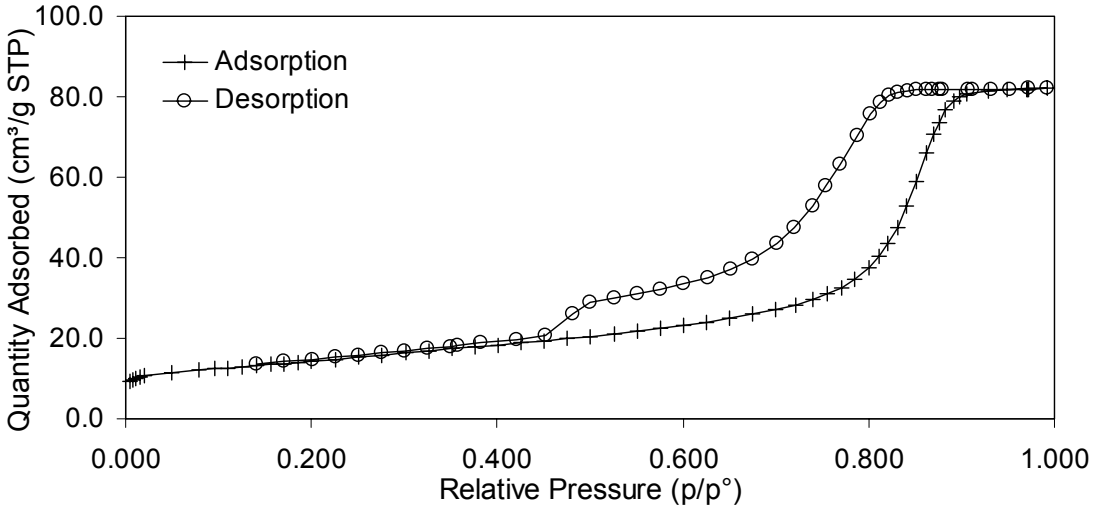

Figure 2.4. Nitrogen adsorption (+)-desorption (O) isotherms of the mesoporous ceramic after heat treatment to 1500 °C. STP, standard temperature and pressure.

In summary, we have demonstrated that when the block copolymer PI-*b*-PDMAEMA is employed as a structure-directing agent for Ceraset, a precursor for high-temperature ceramics, a nanocomposite with hexagonal morphology is obtained. High temperature treatment up to 1500 °C under nitrogen results in a mesoporous ceramic with open and accessible pores. To the best of our knowledge, this is the first

time an ordered mesoporous high temperature ceramic material has been obtained through a block copolymer type bottom-up approach. This exciting result has the potential to open a new field for the generation of nanostructured high-temperature ceramics with novel property profiles.

Acknowledgment

This work was funded by the Gates Millennium Fellowship (CG), the National Science Foundation (DMR-0312913), and the Cornell Center for Materials Research (CCMR) (DMR-0079992). The work made use of the Cornell Center for Materials Research X-ray diffraction facility, the Hudson mesoscale facility, and the electron and optical microscopy facility, all supported through the National Science Foundation Materials Research Science and Engineering Centers Program (DMR-0079992). We also thank Ruediger Dieckmann, Hongxia Lu, Surbhi Mahajan, Sabine Renker, and Yuanming Zhang for help in synthesis and characterization.

REFERENCES

[1] C. T. Kresge, M. E. Leonowicz, W. J. Roth, J. C. Vartuli, J. S. Beck, *Nature* **1992**, *359*, 710.

[2] C. G. Göltner, M. Antonietti, *Adv. Mater.* **1997**, *9*, 431.

[3] D. Zhao, J. Feng, Q. Huo, N. Melosh, G. H. Fredrickson, B. F. Chmelka, G. D. Stucky, *Science* **1998**, *279*, 548.

[4] M. Templin, A. Franck, A. Du Chesne, H. Leist, Y. M. Zhang, R. Ulrich, V. Schädler, U. Wiesner, *Science* **1997**, *278*, 1795.

[5] P. Yang, D. Zhao, D. I. Margolese, B. F. Chmelka, G. D. Stucky, *Nature* **1998**, *396*, 152.

[6] C. B. W. Garcia, C. Lovell, C. Curry, M. Faught, Y. M. Zhang, U. Wiesner, *J. Polym. Sci. B: Polym. Phys.* **2003**, *41*, 3346.

[7] R. L. K. Matsomoto, *Mater. Res. Soc. Symp. Proc.* **1990**, *180*, 797.

[8] S. Creutz, P. Teyssié, R. Jérôme, *Macromolecules* **1997**, *30*, 6.

[9] P. F. W. Simon, R. Ulrich, H. W. Spiess, U. Wiesner, *Chem. Mater.* **2001**, *13*, 3464.

[10] I. W. Hamley, *The Physics of Block Copolymers*; Oxford University Press: Oxford, UK, **1998**.

[11] S. Brunauer, L. S. Deming, W. S. Deming, E. Teller, *J. Am. Chem. Soc*. **1940**, *62,* 1723.

[12] E. P. Barrett, L. G. Joyner, P. P. Halenda, *J. Am. Chem. Soc.* **1951**, *73*, 373.

[13] S. R. Shah, R. Raj, *Acta Mater.* **2002**, *50*, 4093.

CHAPTER 3

COMPOSITION AND MORPHOLOGY CONTROL IN ORDERED MESOSTRUCTURED HIGH TEMPERATURE CERAMICS FROM BLOCK COPOLYMER MESOPHASES[2]

Abstract

In this paper the process of co-assembly is investigated between a poly(isoprene–*block*–dimethylamino ethylmethacrylate) (PI–*b*–PDMAEMA) block copolymer, as the structure directing agent, and a poly(ureamethylvinyl)silazane (PUMVS). In studies of hybrid compositions it is demonstrated that PUMVS is susceptible to reaction with water leading to a replacement of nitrogen by oxygen, which can be circumvented by working under dry conditions. The hybrid morphology can be controlled by systematically increasing the inorganic/organic ratio or by changing the molecular weight of the block copolymer. Temperature treatment up to 1500°C of the hybrids resulted in mesoporous, ordered non-oxide-type ceramics. The results suggest that careful control of co-assembly processes enable access to nanostructured high-temperature ceramics that may have novel mechanical, thermal and chemical properties.

[2] Kamperman, M.; Du, P.; Scarlat, R. O.; Herz, E.; Werner-Zwanziger, U.; Graf, R.; Zwanziger, J. W.; Spiess, H. W.; Wiesner, U. *Macromolecular Chemistry and Physics* **2007**, *208*, 2096-2108.

Introduction

Ordered mesostructured ceramic materials have a wide variety of potential applications ranging from fuel cell membranes to molecular filtration to catalyst supports. However, the ability to form mesostructured ceramics by conventional ceramic processing is limited by the lack of suitable building blocks of the right size and monodispersity. To overcome these challenges Mobil Corporation pioneered the use of molecular surfactants to template inorganic precursors to make ordered mesoporous aluminosilicates [1] Similarly, amphiphilic block copolymers have been shown to direct the structure of metal oxides into a variety of mesophases through interactions between the inorganic precursors and the organic amphiphile, thereby extending the accessible pore diameters to tens of nanometers not readily accessible using molecular surfactants [2-4]. The inorganic components are selectively added to one of the blocks, thereby swelling it. Different mesophases are observed by systematically increasing the inorganic to block copolymer weight fraction. In the meantime, this approach has been extended towards several blocked macromolecular amphiphiles, towards co-assembly of several types of inorganic particles and towards thin films [5].

Beyond producing mesostructured oxides, it is an interesting challenge to generalize the block copolymer approach towards high temperature polymer-derived ceramics because of their excellent thermal and mechanical properties [6,7]. As the name suggests, these materials start out as polymers, which can be easily shaped into complex structures. Heat treatment transforms the polymeric precursors into ceramic materials, while retaining the original (complex) shape. Thus, these materials have a polymer-derived structure and ceramic-like properties. In this way, unconventional structures such as fibers, coatings and microelectronic mechanical systems (MEMS) can be produced [8-10]. Since the start of the development of polymer derived

ceramics in the 1970s [11], a wide variety of silicon-containing compounds have been examined, of which the silicon-based non-oxides (Si_3N_4, SiC, SiN_xC_y, or Si_3N_4-SiC compounds) received the most attention because of their materials properties. More recently polymer derived ceramics were used for the synthesis of porous SiC and SiN_xC_y materials, using a polystyrene or silica template [12,13].

The combination of the two initially separate research areas of block copolymer mesophase formation and polymer derived ceramics enables the synthesis of ordered mesoporous high temperature ceramics. To this end we first showed that the amphiphilic diblock copolymer poly(isoprene–*block*–ethylene oxide) (PI–*b*–PEO) can serve as a structure directing agent for poly(ureamethylvinyl)silazane (PUMVS), commercially known as Ceraset [14]. In 2004 we demonstrated, to the best of our knowledge for the first time, that mesoporous high temperature ceramic materials stable up to 1500 °C can be prepared based on a related approach using poly(isoprene–*block*–dimethylamino ethylmethacrylate) (PI–*b*–PDMAEMA) as the structure directing agent for PUMVS [15]. Both the molecular structure of the block copolymer and the preceramic polymer, as well as details of the heat treatment to convert the liquid PUMVS precursor to a ceramic are shown in Figure 3.1. In the meantime similar results have been produced with polybutadiene-*block*-poly(ethylene oxide) (PB-*b*-PEO) as the structure directing agent [16,17]. Furthermore, the same group recently developed a method to obtain nanoordered high temperature ceramics directly, by introducing a single-source ceramic precursor, which is a block copolymer of polynorbornene-decaborane (PNB-*b*-PDB30) [18].

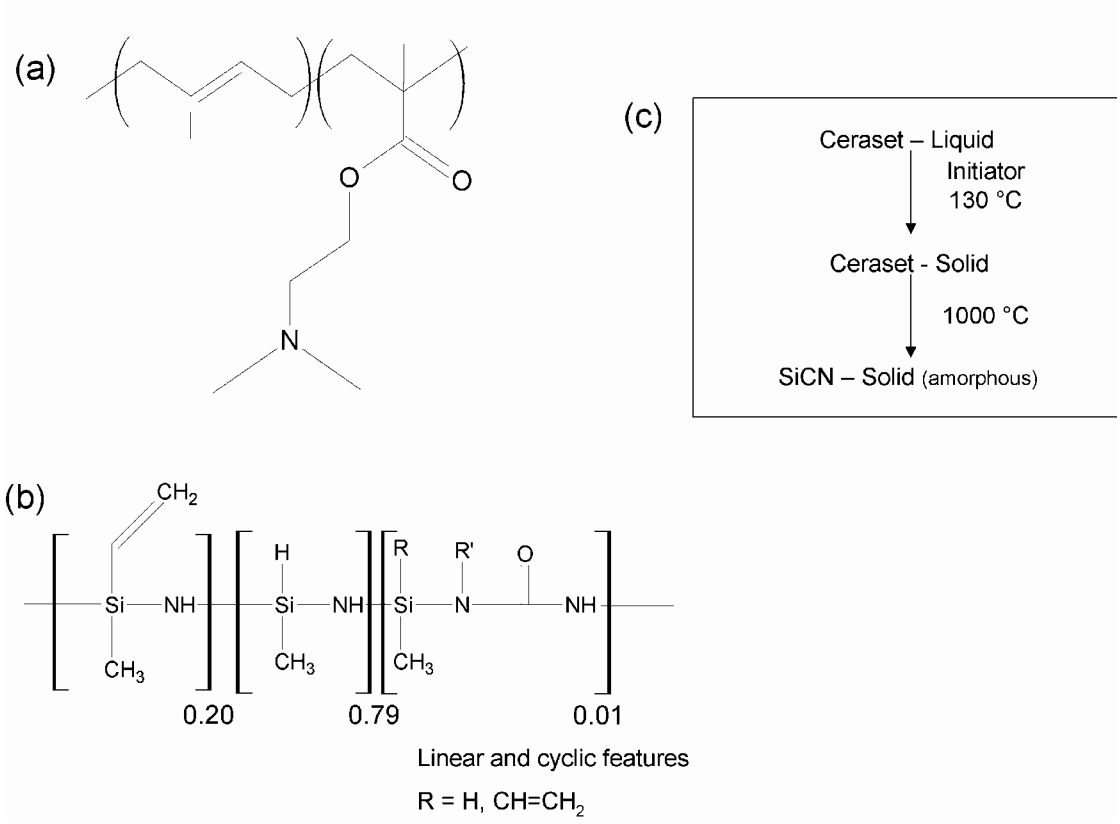

Figure 3.1. Chemical structure of (a) poly(isoprene–*block*–dimethylamino ethyl methacrylate) and (b) poly(ureamethylvinyl)silazane (PUMVS). No information is available about the R'. (c) Details of the heat treatment of PUMVS resulting in amorphous SiCN [6].

In this paper a full account of the results on PI–*b*–PDMAEMA as a structure directing agent for PUMVS is given. We provide a detailed description of the synthesis of the hybrid materials as well as their conversion into ordered ceramic materials. We describe that in order to obtain non-oxide type ceramics the PUMVS, which reacts with water, must be kept away from all sources of moisture. The compositional changes are investigated with solid state NMR and Rutherford Back Scattering (RBS). Furthermore we show that various morphologies with variable lattice spacings are accessible for composites with PUMVS including the inverse hexagonal morphology from which mesoporous non-oxide type ceramics stable up to

1500° C are obtained. Sample morphologies are characterized using a combination of Small Angle X-ray Scattering (SAXS) and Transmission Electron Microscopy (TEM). We finally demonstrate that dissolution of hybrids with morphologies rich in PI may pave the way towards high temperature ceramic nanoparticles with well controlled shape and size.

Experimental Part

Materials Preparation

The block copolymer PI–*b*–PDMAEMA was polymerized by anionic polymerization as described elsewhere [19,20]. Gel permeation chromatography (GPC) was used to determine the molecular weight of the first block (polyisoprene, PI) and the polydispersity of the block copolymer. ^{1}H NMR was used to determine the microstructure of the PI block and the chemical composition of the block copolymer. The results were used to determine the overall molecular weight of the block copolymer. The resulting polymers had molecular weights in the range of 19 – 107 kg/mol and 10 – 33 wt.-% PDMAEMA with a polydispersity below 1.2, see Table 3.1. On average 6% of the polyisoprene was 3,4-polyisoprene and 94% was 1,4-polyisoprene.

The synthesis of the mesostructured hybrids was performed by a one-pot synthesis, in which the ceramic precursor is expected to swell the PDMAEMA block [15]. The ceramic precursor, Ceraset (KiON Corp.) and the radical initiator, dicumyl peroxide (Aldrich) were used as received. The chemical structures of block copolymer and the PUMVS are shown in Figure 3.1. In a typical synthesis under dry conditions, a 5 wt.-% block copolymer solution in anhydrous toluene was mixed with the ceramic precursor and the radical initiator (1 wt.-% with respect to the mass of PUMVS added) and stirred inside the glove box for 1h. The solution was subsequently poured into a

Petri dish under dry conditions and a film cast by solvent evaporation in an oven at 50 ºC followed by annealing for 24 h under vacuum. This resulted in a film thickness of about 500 μm. Care was taken to insure the previous steps were performed under a nitrogen atmosphere. The temperature was then increased to 130 ºC for 3 h to crosslink the PUMVS. The composite was finally heat treated using 1 ºC/min ramps under argon(95%)/hydrogen(5%) up to temperatures as high as 1500 ºC for conversion into the high-temperature ceramic material. In a typical synthesis under ambient atmosphere THF was used as a solvent. A glove box was not used and all steps were performed under ambient atmosphere (i.e., not under nitrogen atmosphere). Nanoobjects with different shapes and sizes were obtained by dissolving 5 mg of mesostructured hybrids in 10 mL of THF.

Table 3.1. Characterization of PI-*b*-PDMAEMA block copolymers

Block copolymer	**MW PI-*b*-PDMAEMA (g/mol)**	**Polydispersity**	**wt.-% PDMAEMA**
A	107 200	1.18	10
B	19 100	1.09	26
C	31 100	1.05	33

Gel Permeation Chromatography (GPC)

Measurements were performed in 98% tetrahydrofuran (THF) and 2% N,N-dimethylacetamide at room temperature using 5 μm Waters Styragel columns (103, 104, 105, 106 Å, 30 cm each; Waters Corporation, Milford, MA) at a flow rate of 1.0 mL/min. A Waters 490 programmable multi-wavelength UV diode array detector (operated at λ= 260 nm) and a Waters 410 RI detector operated at 25 °C were used.

Raw data were processed using PSS-Win GPC V6.2 (Polymer Standards Service, Mainz, Germany) software.

Microprobe

Experiments were performed on a JEOL 8900 EPMA equipped with five automated Wavelength Dispersive X-Ray Spectrometers (WDS). The microprobe was operated at 18.5 nA, 5kV and a beam diameter of 0.75 μm. The standards chosen for WDS were quartz for Si and O, BN for N, and calcite for C. The crystals were TAP for Si (2d = 25.757 Å), LDE1H for O (2d = 60 Å) and N and LDE4H (2d = 120 Å) for C.

^{1}H, ^{13}C and ^{29}Si Nuclear Magnetic Resonance (NMR)

^{1}H, ^{13}C and ^{29}Si solution NMR spectra were recorded on Varian INOVA 400 and 500 MHz spectrometers using $CDCl_3$ signal as an internal standard for ^{1}H (δ = 7.27 ppm) and ^{13}C (δ = 77 ppm). TMS was used as an external standard for ^{29}Si NMR (δ = 0 ppm). ^{29}Si and ^{13}C solid state magic angle spinning (MAS) NMR studies were performed on a Bruker Avance NMR spectrometer with a 16.45 Tesla magnet. For the ^{29}Si NMR spectra the samples were spun in rotors with 4mm diameter at 10 kHz. The ^{29}Si NMR spectra were acquired with cross-polarization and spinal-64 decoupling [21] using 5ms contact times and 2s recycle delays for typically 3600 scans. The ^{29}Si chemical shift scale was referenced against the Kaolin resonance at -91.3 ppm. For ^{13}C NMR measurements the samples were spun in rotors of 2.5mm diameter at 10 kHz and at 12 kHz to identify spinning sidebands. The carbonyl resonance of glycine at 176.03 ppm served as external chemical shift reference. Cross-polarization with 4ms contact times, spinal-64 decoupling and 5s recycle delays were used to acquire typically 2880 scans.

Rutherford Backscattering (RBS)

Silicon wafers were used as purchased from the Cornell Nanofabrication Facility. Thin films (about 0.2 μm) were fabricated by combining an amount of copolymer with 2 times the amount (by weight) PUMVS and 0.5 wt.-% (w.r.t. PUMVS) dicumyl peroxide in THF or toluene (4 wt.-% total solution) and spin coated onto silicon wafers at 2000 rpm at 250 rpss for a total of 1 minute in ambient atmosphere. Samples fabricated in the nitrogen glovebox (from a similar solution) were processed on a makeshift spin coater (made from a 12V cooling fan motor) at 4000 rpm (uncontrolled acceleration) for a total of 1 minute. Glovebox samples were mounted onto a RBS holder and sealed in a media bottle before removal into the ambient atmosphere. All samples were annealed in a vacuum oven at 130 ° C for 1 h to crosslink the PUMVS and permanently set the thin films. RBS measurements were taken with a 1.96 MeV He^{++} beam, 163.9° detection angle, 40μC dosage. Energy calibration was accomplished through the use of a TaSi standard.

Small Angle X-Ray Scattering (SAXS)

Experiments were performed on a Bruker-AXS NanoSTAR and at the Cornell High Energy Synchrotron Source (CHESS). The Bruker-AXS NanoSTAR setup consisted of an X-ray source (CuK_{α}, 1.54 Å) operated at 40 kV, 40 mA in transmission mode. Göebbel mirrors were used to focus the beam. A 2-D Hi-Star area detector at a sample-to-detector distance of 62.5 cm was used to record the scattering images. 2D images were integrated over the azimuthal angle (μ) to obtain one-dimensional intensity vs scattering plots. The SAXS data obtained at CHESS were collected with a CCD 2-D detector operating at X-ray energy of 1.242 Å, sample-to-detector distance of 145.5 cm and exposure times of 1-20 sec.

Transmission Electron Microscopy (TEM)

Samples were sectioned ultrathin with a Leica Ultracut UCT microtome at -60 ºC for composites and at room temperature for ceramics. Bright field TEM micrographs were taken on a LEO 922 EFTEM operating at 200 kV.

Results and Discussion

We report on the preparation of mesoporous high temperature ceramic materials using PI–*b*–PDMAEMA as a structure directing agent for a polymeric ceramic precursor, poly(ureamethylvinyl)silazane (PUMVS). Blending PUMVS with the block copolymer is expected to lead to preferential segregation of the PUMVS within the PDMAEMA domains primarily due to the polar nature of the molecule (see Figure 3.1). This increases the effective volume fraction of the PDMAEMA domains. Different mesophases similar to those in block copolymer/homopolymer mixtures should thus be accessible by systematically increasing the PUMVS to block copolymer weight fraction. This situation can be compared to that encountered in studies of an epoxy resin embedded in one phase of a block copolymer [22,23]. The structure is permanently set by crosslinking the PUMVS with a radical initiator.

Studies of Hybrid Composition

Initially the hybrid samples were prepared by dissolving all the components in THF, followed by casting a film (about 500 μm) in a Petri dish placed on a hotplate in ambient atmosphere. Preliminary microprobe results showed, however, that the chemical composition of the hybrid films was drastically altered during the preparation. Instead of materials composed of mainly Si, H, C, and N atoms, as expected from the starting materials, hybrids with a composition of Si, H, C, and O atoms were obtained. There are two obvious possible sources for the additional

oxygen within the hybrid sample: reaction with water or molecular oxygen. Literature suggests that the Si–N bond within the PUMVS is susceptible to attack by water, whereas molecular oxygen is not mentioned [24]. Following this argument, the Si–N bond is attacked by water forming Si–OH bonds. The hydroxy groups can subsequently condense to form Si–O–Si bridges and a molecule of ammonia is eliminated. Moreover, in light of this suggested mechanism, the hygroscopic nature of THF would render it an unsuitable solvent for this system. In order to study these effects a series of experiments were performed. First, ^{1}H, ^{13}C and ^{29}Si NMR solution spectra were obtained on the PUMVS polymer and ^{1}H NMR spectra of the block copolymer to verify molecular structure, in particular for the polymer provided by the company to make sure that it had not degraded or reacted in any way. Second, Rutherford Backscattering (RBS) experiments on thin films were performed to determine the source of the water and at which step it reacts with the hybrid sample. Finally, ^{1}H, ^{13}C and ^{29}Si solid state NMR experiments were performed on two film samples of crosslinked PUMVS to gain insight into the compositional changes due to moisture.

^{1}H, ^{13}C and ^{29}Si NMR solution spectra

The NMR spectra of PUMVS as well as the ^{1}H NMR spectra of the block copolymer, PI–*b*–PDMAEMA, are shown in Figure 3.2. $CDCl_3$ was used as a solvent to obtain all spectra. The PUMVS ^{1}H NMR spectrum in (a) shows four groups of peaks. These can be assigned to Si-CH_3 (0.09 ppm), N-H (0.70 ppm), Si-H (4.24–4.80 ppm) and SiCH=CH_2 (5.54–6.14 ppm) [6]. The ratios of the CH_2=CHSi, H-Si, and CH_3-Si units were determined from the respective peak intensities to be 1:1.3:4.3, which is in reasonable agreement with the molecular structure provided by the KiON Corporation, company corresponding to a ratio of 1:1.3:5. The PUMVS ^{13}C NMR

spectrum in (b) shows two groups of peaks, which were assigned to Si-CH_3 groups (-2.5–4.7 ppm) and CH_2=CH (137.2–141.8 and 130.3–133.1 ppm) [6]. There was no signal from the C=O groups detected, presumably because these groups are part of the repeating unit that only constitutes 1% of the PUMVS molecule and therefore this signal is too weak to be detected. The PUMVS ^{29}Si NMR spectrum in (c) shows one broad group of peaks (-15– -25 ppm), which are assigned to CH_3HSiN_2 and CH_3CH_2=$CHSiN_2$ [6]. All NMR results are thus consistent with the molecular structure provided by KiON. Furthermore, the ^{1}H NMR spectrum of the block copolymer is also consistent with expectations, as shown in Figure 3.2(d) [19].

Rutherford Backscattering experiments on thin films

RBS experiments were performed to determine the source of the water and at which step it reacts with the hybrid sample. Thin films were created by spin coating various solutions of PI–*b*–PDMAEMA, PUMVS, and dicumyl peroxide initiator on silicon substrates, see Table 3.2. Several different methods of elemental analysis were initially explored, but RBS was chosen due to the ease of sample preparation and straightforward interpretation of the data. Most importantly, the depth profiling nature of RBS allows for the study of elemental concentrations as a function of film depth, an especially powerful tool when dealing with reactions at interfaces and surfaces.

The RBS spectrum obtained from sample I, which contains the block copolymer and initiator but lacks the ceramic precursor in THF, is shown in Figure 3.3a. The spectrum has the characteristic profile of an organic thin film on a silicon wafer, namely light element peaks on a plateau from a heavier element substrate. This particular sample establishes the baseline for comparison to later samples with the PUMVS, in particular the amount of lighter elements (C, N, and O) contained within the hybrid material. Note that hydrogen cannot be detected with RBS, because the

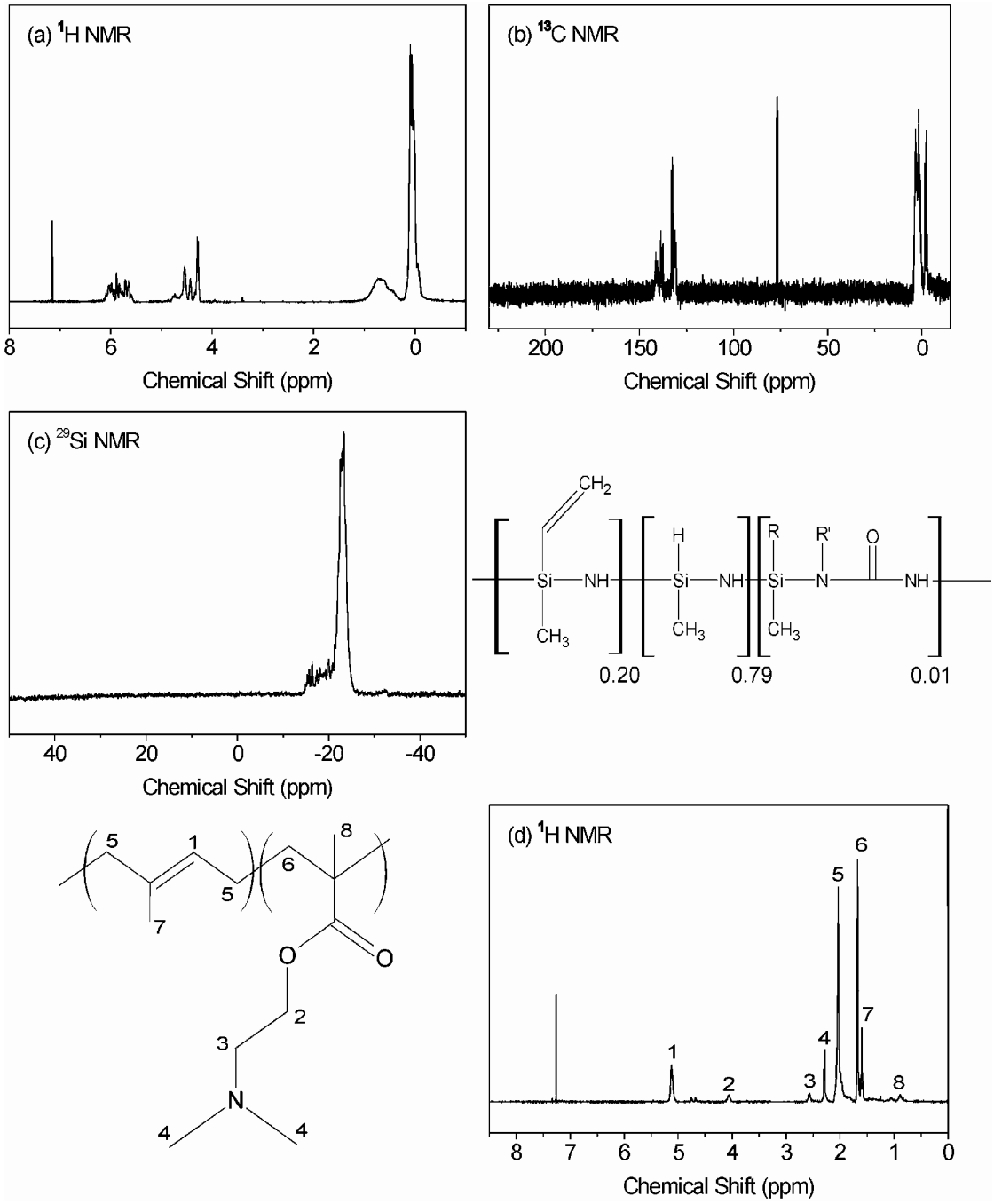

Figure 3.2. (a) ^{1}H, (b) ^{13}C and (c) ^{29}Si NMR spectra of the PUMVS polymer. $CDCl_3$ is used as a solvent for all the spectra. Note: different batches of the PUMVS from the supplier don't show any differences in any of the spectra. (d) ^{1}H NMR spectra of PI–*b*–PDMAEMA in $CDCl_3$.

Table 3.2. Details of hybrid material fabrication conditions.

sample	materials	geometry	atmosphere	relative humidity (%)	temperature (°C)
I	PI–*b*–PDMAEMA, dicumyl peroxide, THF	thin film	ambient	40-60	20
II	PI–*b*–PDMAEMA, dicumyl peroxide, PUMVS,THF	thin film	ambient	40-60	20
III	PI–*b*–PDMAEMA, dicumyl peroxide,PUMVS, toluene	thin film	ambient	40-60	20
IV	PI–*b*–PDMAEMA, dicumyl peroxide, PUMVS, toluene	thin film	nitrogen	0	20
V	PUMVS, dicumyl peroxide	film	nitrogen	0	50
VI	PUMVS, dicumyl peroxide, THF	film	ambient	40-60	50
VII	PI–*b*–PDMAEMA, dicumyl peroxide, PUMVS, toluene	film	nitrogen	0	50
VIII	PI–*b*–PDMAEMA, dicumyl peroxide, PUMVS,THF	film	ambient	40-60	50

* All samples are heat treated to 130 °C after initial spincoating/casting to crosslink the PUMVS.

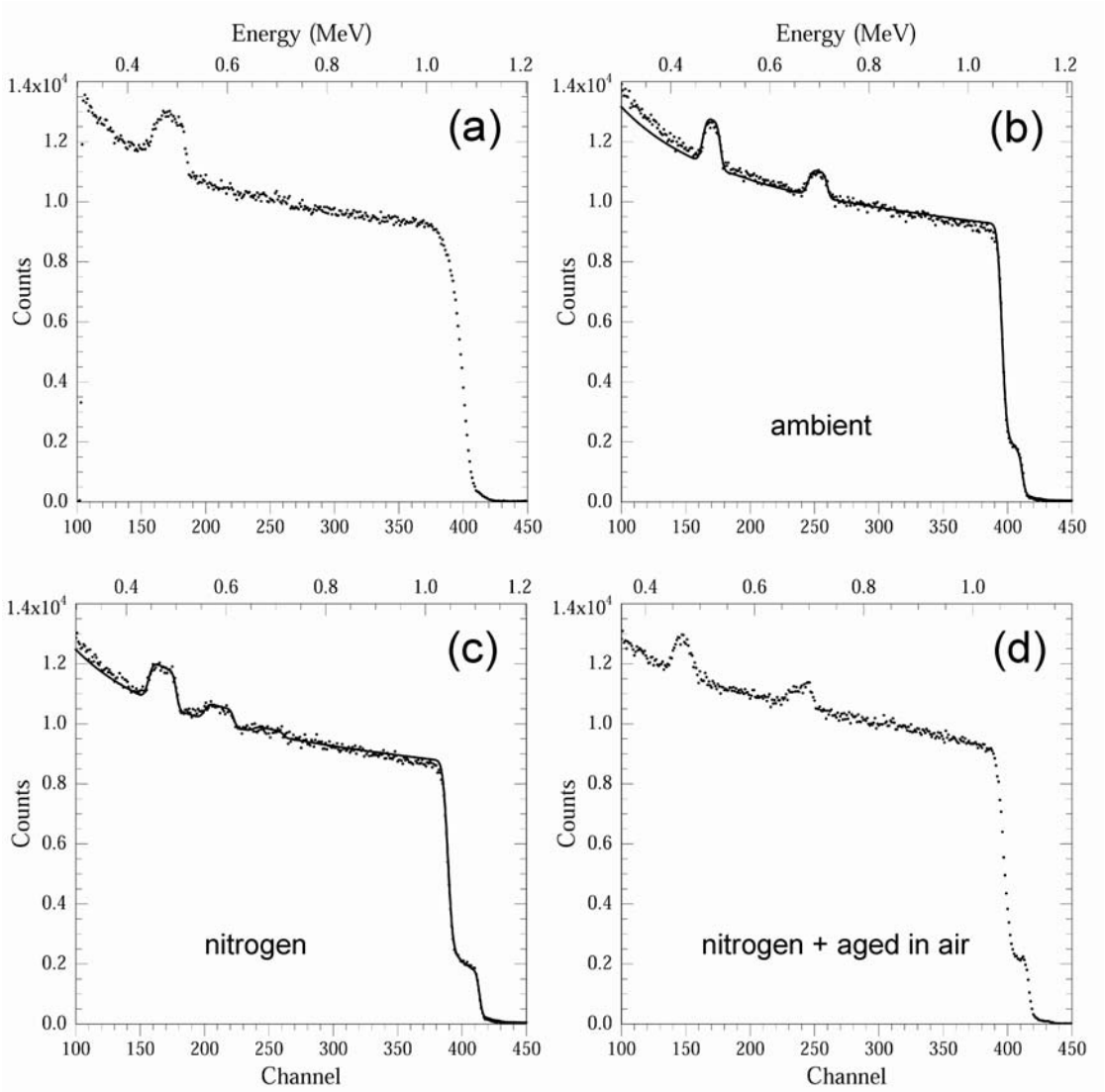

Figure 3.3. RBS spectra of thin films. The shoulder and peaks are indexed with their elemental abbreviations. a) Sample I (polymer, initiator, THF), b) Sample II (polymer, initiator, PUMVS, THF), c) Sample IV (polymer, initiator, PUMVS, toluene), and d) from a sample similar to IV, but aged in air. Simulations from the RUMP software are overlaid in solid black for Samples II and IV.

mass of the incident particle is greater than that of the hydrogen atom and therefore the particles are not scattered in a backward direction in elastic collisions. The single peak on the silicon substrate confirms that carbon is the major component in thin film sample I. Next, hybrid materials fabricated from the inorganic precursor were characterized. The RBS spectrum for hybrid sample II (polymer, initiator, and PUMVS) in THF is shown in Figure 3.3b. The shoulder starting at channel 420 represents the silicon contribution from the PUMVS in the thin film. The two lower energy peaks represent carbon and oxygen at channels 180 and 270, respectively. Comparison of the RBS spectra of samples I and II suggest that the new features result from the PUMVS in the polymer solution. Theoretical calculation of the chemical composition for this hybrid material based on the composition of the starting materials is shown in Table 3.3. Inspection of the RBS spectrum shows the silicon signal as expected, but the absence of nitrogen and abundance of oxygen suggest chemical conversion occurring during hybrid mixture processing.

Table 3.3. Elemental characteristics in weight percentage. Sample II and Sample IV are analyzed using RBS, whereas the heat treated sample is analyzed with a microprobe.

Sample	Preparation	Si	O	N	C
	theoretical	31.89	2.13	16.92	49.06
II	ambient atmosphere	25.40	21.64	-	52.95
IV	dry nitrogen atmosphere	27.08	4.60	18.14	50.18
	heated to 1500 °C under Ar/H_2	29.0	8.7	30.4	31.8

The relative chemical stability of the different components suggests that the chemical conversion should not occur within the PI–*b*–PDMAEMA copolymer. This is supported by the lack of an oxygen signal in the RBS spectrum of sample I, even after aging of the thin film (data not shown). Although a chemical conversion most likely involves the PUMVS, the source of the excess oxygen and the mechanism of its introduction required further experiments. The synthesis of hybrid sample III was carried out in toluene in an attempt to limit the amount of water introduced through the solvent. The RBS spectrum of sample III (data not shown) contains the silicon shoulder and carbon and oxygen peaks similar to spectrum II, and there is still a conspicuous absence of any nitrogen signal. Due to the low solubility of water in toluene, this result suggests that the PUMVS in the thin film is reacting with moisture from the atmosphere.

To isolate the thin film from atmospheric moisture, synthesis of sample IV was carried out in a nitrogen glovebox (see Experimental Section and Table 3.2). The sample was sealed in a media bottle prior to removal from the glovebox and loaded into the RBS chamber with minimal exposure to the atmosphere. The RBS spectrum of sample IV is shown in Figure 3.3c. The silicon shoulder and carbon peak are similar to all other spectra from PUMVS-containing samples (see Figure 3.3b). The obvious differences are the appearance of a nitrogen peak and the suppressed oxygen signal. This is in agreement with the suggested mechanism of the Si–N to Si–O conversion, by way of hydrolysis and condensation. Furthermore, the spectrum of sample IV converts to one that is similar to that of sample III with aging of the film under ambient atmosphere (see Figure 3.3d), suggesting that moisture in the air is indeed responsible for the reaction of the Si–N bond. Further supporting data comes from the RBS spectrum of a pure PUMVS/initiator film fabricated in the glovebox and

transferred via sealed media bottle. This spectrum shows an enrichment of oxygen at the surface of the film (data not shown), strongly suggesting that the attack starts at the film-air interface.

The qualitative data interpretation is corroborated by quantitative analysis. Simulations of RBS spectra were created with RUMP [25] software to help determine the chemical composition of these hybrid thin film samples, see Table 3.3. The simulated spectra (solid line) are overlaid on the experimental data (circles) shown for sample II and IV in Figures 3.3b and c, respectively. Simulated spectra for the films fabricated under ambient atmosphere, samples II and III, contain the expected amount of silicon and carbon, but elevated amounts of oxygen (see Figure 3.3b). However, the complete replacement of the nitrogen accounts for this excess oxygen. This further supports the mechanism of oxidation of the Si–N bond. The simulation for sample IV provides a composition that reasonably matches with the theoretical composition (see Figure 3.3c).

^{1}H, ^{13}C and ^{29}Si solid state NMR spectra

^{1}H, ^{13}C and ^{29}Si solid state NMR experiments were performed on two film samples (thickness about 500 μm) of crosslinked PUMVS to gain insight into the compositional changes in thicker films due to moisture. Sample V was prepared by crosslinking a mixture of PUMVS and radical initiator inside a nitrogen glovebox and sample VI was prepared by dissolving PUMVS and the radical initiator in THF (used as received), casting a film and crosslinking the sample on a hotplate under ambient atmosphere. The NMR results on these samples are shown in Figure 3.4 and are summarized in Table 3.4. The results show that, while the carbon spectra differ somewhat between the two samples, the silicon spectra show the most significant changes. The ^{1}H NMR spectra for both samples show the same peaks and have some

peaks in common with the ^{1}H NMR spectrum for the non-crosslinked PUMVS (see Figure 3.2). This is expected, because crosslinking is due to vinyl group polymerization leaving the Si–CH_3 (0 ppm), N–H (0.8 ppm) and the Si-H groups (4.5 ppm) unreacted and therefore at the same spectral position for all ^{1}H NMR spectra. The spectra show two small peaks at 6 ppm and 7 ppm assigned to unreacted SiCH=CH_2 and aryl groups in the dicumyl peroxide, respectively. The ^{13}C CP-MAS NMR spectra for both samples show a group of peaks around 0 ppm, which can be assigned to the Si-CH_3, SiCH$(CH_2)_2$ groups [6]. The spectrum of the dry sample

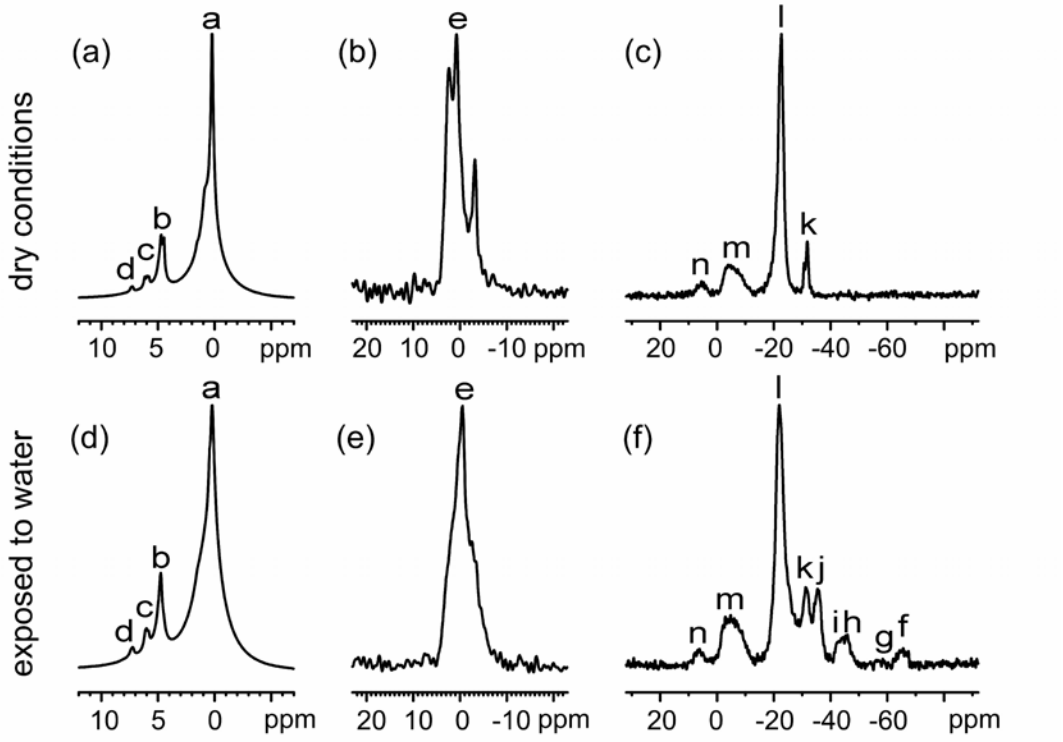

Figure 3.4. (a) ^{1}H, (b) ^{13}C and (c) ^{29}Si Solid State NMR spectra of a crosslinked PUMVS sample that is crosslinked under dry conditions (Sample V). (d) ^{1}H, (e) ^{13}C and (f) ^{29}Si NMR spectra of a crosslinked PUMVS sample that is exposed to water during crosslinking (Sample VI).

shows significantly better resolution, suggesting that polymerization in ambient conditions may generate a more disordered local environment. The peaks of the vinyl groups are not observed anymore, whereas some unreacted SiCH=CH_2 groups were

observed in the hydrogen spectrum, probably due to the reduced signal-to-noise ratio of the ^{13}C CP-MAS NMR spectra. The ^{29}Si CP-MAS spectrum for the sample that is crosslinked under dry conditions (sample V) shows four peaks. The broad peak around 0 – -10ppm and the intense peak at -21 ppm were expected and can be assigned to C_2–Si–N_2 and CH_3–HSi–N_2, respectively [6]. The small peak at 7 ppm is assigned to C_3-Si-N groups and the peak at -30 ppm to $CH_2(CH_3)SiON$ groups. C_3-Si-N groups are formed from Kumada-like rearrangement reactions that occur during cross-linking [26,27]. The ^{29}Si CP-MAS spectrum for the sample that is crosslinked under ambient atmosphere (sample VI) deviates more from the expected spectrum and shows eight peaks. The first four peaks at 7, 0 – -10, -21 and -30 ppm are the same as for the other sample and can be assigned to the same groups. The additional peaks at -35, -45, -53 and -65 ppm can be assigned to $H(CH_3)SiON$, $H(CH_3)SiO_2$/ $CH_2(CH_3)SiO_2$, $(CH_3)SiO_2(OH)$ and CH_3SiO_3 silicon environments, respectively, in agreement with solid state NMR data on silicon oxycarbides known from literature [28-30].

The results corroborate the suggestion that the Si–N bonds are attacked by water, forming Si–OH bonds that convert to Si–O–Si bridges, evolving a molecule of ammonia in the process. In this scenario all the Si–N bonds of PUMVS can be attacked, which implies that all silicon atoms can be bonded to at most two oxygen atoms (see PUMVS structure in Figure 3.1(b)). The peak at -65ppm, however, indicates silicon atoms bonded to three oxygen atoms in the hybrid materials. This suggests that in addition to the Si-N bond, the Si-H bond is attacked as well. The relative decrease in intensity of the CH_3-HSi-N_2 groups at -22 ppm corroborates this reaction path. The fact that the spectra of the sample prepared under dry conditions also shows a peak at -30 ppm ($CH_2(CH_3)SiON$) can be explained by the fact that the NMR experiments were not performed right after the synthesis of the samples. In the

period between synthesis and measurement the crosslinked film may have reacted with some source of moisture.

Table 3.4. Assignments for ^{1}H, ^{13}C and ^{29}Si Solid State NMR spectra for a crosslinked PUMVS sample that is exposed to water during crosslinking and for a sample that is crosslinked under dry conditions.

	Exposure to water [6, 9, 28]		**Dry conditions [6, 30]**	
	ppm		ppm	
^{1}H NMR	0 4.5 5.8 7.0	**a** Si-C**H**$_3$, Si-N**H**-Si, SiC**H**(C**H**$_2$)$_2$ **b** Si–**H** **c** SiC**H**=C**H**2 (unreacted ceraset) **d** Aryl group from dicumylperoxide	0.2 4.5 5.9 7.1	**a** Si-C**H**$_3$, Si-N**H**-Si, SiC**H**(C**H**$_2$)$_2$ **b** Si–**H** **c** SiC**H**=C**H**2 (unreacted ceraset) **d** Aryl group from dicumylperoxide
^{13}C NMR	-4 – 7	**e** Si – **C**H$_3$, Si**C**H(**C**H$_2$)$_2$	-5 – 5	**e** Si – **C**H$_3$, Si**C**H(**C**H$_2$)$_2$
^{29}Si NMR	-68 - -62 -57 -49- - 41 -35 -31 -22 -12 - 0 7	**f** CH$_3$**Si**O$_3$ **g** CH**Si**O$_2$(OH) **h** H(CH$_3$)**Si**O$_2$, **i** CH$_2$(CH$_3$)**Si**O$_2$ **j** H(CH$_3$)**Si**ON **k** CH$_2$(CH$_3$)**Si**ON **l** CH$_3$–H**Si**–N$_2$ **m** C$_2$–**Si**–N$_2$ **n** C$_3$–**Si**–N	-30 -21 -10 - 0 7	**k** CH$_2$(CH$_3$)**Si**ON **l** CH$_3$–H**Si**–N$_2$ **m** C$_2$–**Si**–N$_2$ **n** C$_3$–**Si**–N

The next set of ^{13}C and ^{29}Si solid state NMR experiments was performed on PI-*b*-PDMAEMA/ PUMVS hybrids to investigate the influence of the block copolymer on

the chemical composition of the hybrids synthesized under varying environmental conditions. Again two samples were prepared, one under dry conditions (sample VII) and the other under ambient atmosphere (sample VIII), in which both the block copolymer PI-*b*-PDMAEMA and PUMVS were dissolved and cast into films to obtain nanocomposites (see Experimental Part). Figure 3.5 shows the ^{13}C and ^{29}Si CP-MAS NMR spectra for both samples and Table 3.5 summarizes the results. The ^{13}C CP-MAS spectra of both samples are again similar and all the peaks are expected and can be assigned to groups in the block copolymer or crosslinked PUMVS [6, 31, 32]. The ^{29}Si CP-MAS spectra for the hybrid samples (VII, VIII) are very similar to the ^{29}Si CP-MAS spectra for the crosslinked PUMVS (V, VI), and show the same trends as a function of synthesis conditions, compare Figures 3.4c and 3.5c (dry conditions; samples V, VII) and Figures 3.4f and 3.5d (ambient atmosphere; samples VI, VIII). The stronger peak intensities of the oxidized Si positions in the hybrid sample point to more strongly hydrolyzed materials, either due to the synthesis or due to the delay between synthesis and solid state NMR analysis.

The similarity in the ^{13}C NMR spectra suggests that the block copolymer does not react with PUMVS (although there is the possibility that certain reactions do not alter the spectra noticeably). Furthermore, it appears from the combined ^{13}C and ^{29}Si NMR data that the block copolymer does not change the reaction of PUMVS with water. The polymer might act as a catalyst for the reaction due to its basic nature, but we didn't investigate the kinetics of the reaction quantitatively. Reactions of a block copolymer with PUMVS were described before by Wan *et al*. where the hydroxy chain ends of the PB–*b*–PEO block copolymer react with PUMVS [16]. This kind of reaction is not expected in the current system, however, since the PI-*b*-PDMAEMA does not contain a hydroxyl end group.

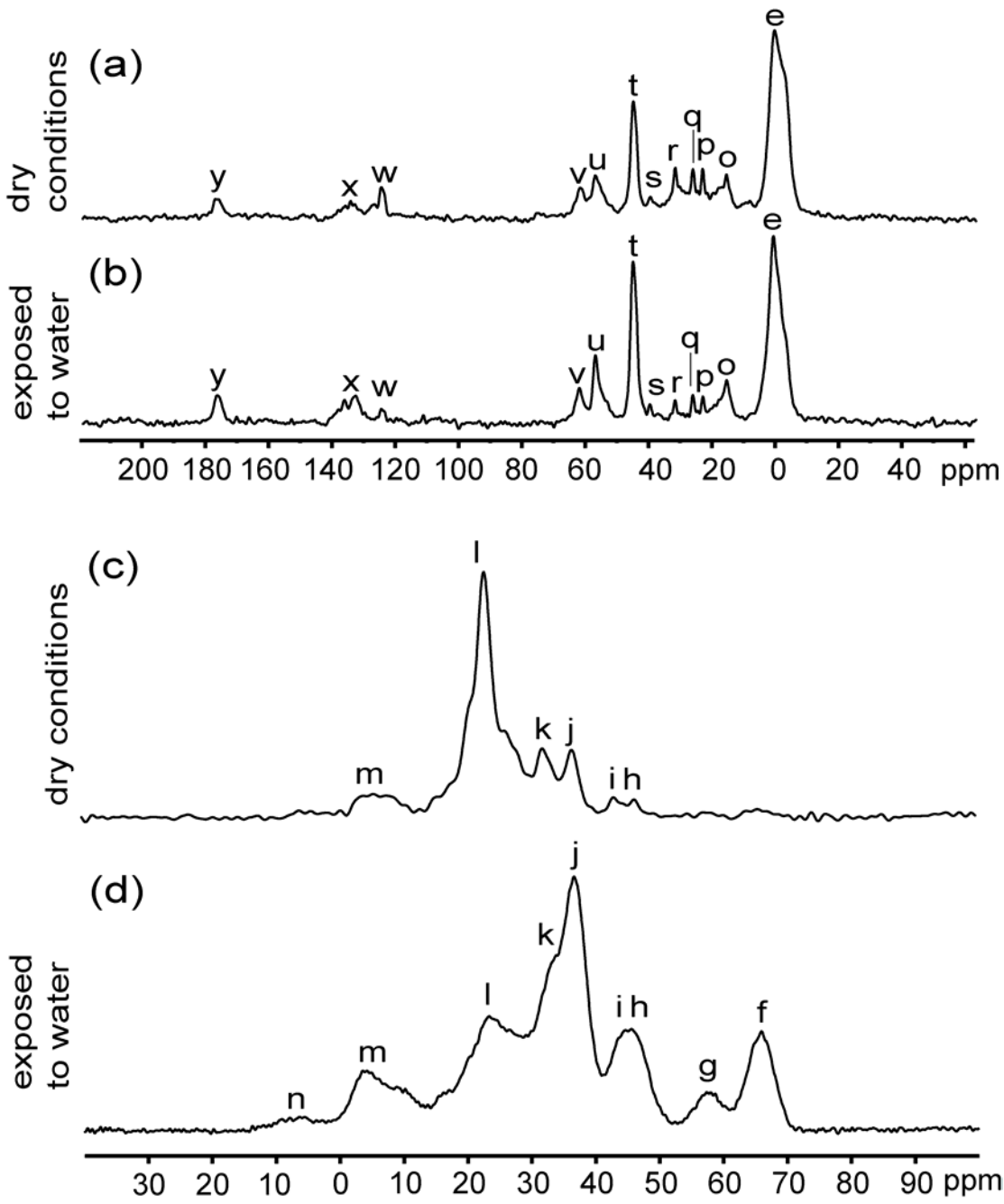

Figure 3.5. (a) ^{13}C and (c) ^{29}Si Solid State NMR spectra of a crosslinked block copolymer PUMVS hybrid sample that is crosslinked under dry conditions (Sample VII). (b) ^{13}C and (d) ^{29}Si NMR spectra of a crosslinked block copolymer PUMVS hybrid sample crosslinked under ambient atmosphere (Sample VIII).

Table 3.5. Assignments for ^{13}C and ^{29}Si Solid State NMR spectra for a crosslinked block copolymer PUMVS hybrid sample that is exposed to water during crosslinking and for a sample that is crosslinked under dry conditions.

Crosslinked PUMVS				**PI-b-PDMAEMA**		
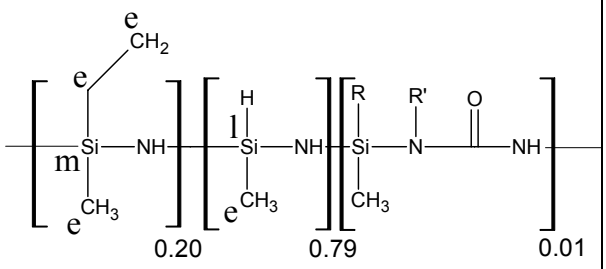				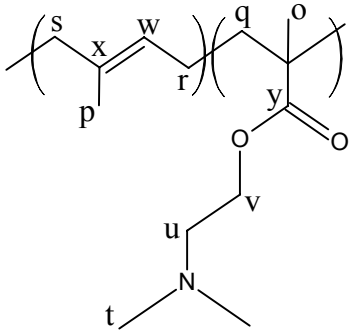		
	Exposure to water			Dry conditions		
	ppm	Crosslinked PUMVS (expected[6])	PI-*b*-PDMAEMA (expected[31, 32])	ppm	Crosslinked PUMVS (expected[6])	PI-*b*-PDMAEMA (expected[31, 32])
^{13}C NMR	1.27	**e** Si – **C**H_3, Si**C**H(**C**H_2)$_2$		1.27	**e** Si – **C**H_3, Si**C**H(**C**H_2)$_2$	
	16.02		**o** – **C**H_3	16.02		**o** – **C**H_3
	23.55		**p** – **C**H_3	23.55		**p** – **C**H_3
	26.71		**q** – **C**H_2	26.71		**q** – **C**H_2
	32.32		**r** – **C**H_2	32.32		**r** – **C**H_2
	40.30		**s** – **C**H_2	40.30		**s** – **C**H_2
	45.59		**t** N– **C**H_3	45.59		**t** N– **C**H_3
	57.48		**u** N – **C**H_2	57.48		**u** N – **C**H_2
	62.53		**v** O – **C**H_2	62.53		**v** O – **C**H_2
	125.10		**w** = **C**H	125.10		**w** = **C**H
	136.73		**x** = **C**	136.73		**x** = **C**
	176.93		**y C** = O	176.93		**y C** = O
	ppm	Crosslinked PUMVS (expected[6, 26, 27])	unexpected[28-30]	ppm	Crosslinked PUMVS (expected[6])	unexpected[28-30]
^{29}Si NMR	-65.95		**f** C-**Si**O_3			
	-57.37		**g** C-**Si**O_2 (OH)			
	-45.58		**h** $CH_2(CH_3)$**Si**O_2	-46.54		**h** $CH_2(CH_3)$**Si**O_2
				-43.31		
	-36.60		**i** $H(CH_3)$**Si**O_2	-36.76		**i** $H(CH_3)$**Si**O_2
			j $H(CH_3)$**Si**ON	-32.15		**j** $H(CH_3)$**Si**ON
	-23.32	**l** CH_3–H**Si**–N_2	**k** $CH_2(CH_3)$**Si**ON	-23.00	**l** CH_3–H**Si**–N_2	**k** $CH_2(CH_3)$**Si**ON
	-3.54	**m** C_2–**Si**–N_2		-5.74	**m** C_2–**Si**–N_2	
	6.34	**n** C_3–**Si**–N				

In summary, the NMR and RBS data are consistent and suggest that PUMVS is susceptible to reaction with water. Not many previous reports regarding PUMVS mention this side reaction. In the present study the prevalence of the enhanced oxygen composition in hybrids prepared under ambient atmosphere may be attributed to the employed (thin) film geometry. This is in agreement with those literature reports that do mention the reactivity with water [13,33]; all of which focus on the synthesis of small scale structures, i.e., structures with large surface-to-volume ratios.

Studies of Hybrid Morphology

Now that we have established how to control the chemical composition of the PI-*b*-PDMAEMA/ PUMVS hybrids we subsequently want to demonstrate that several morphologies can be obtained by systematically increasing the inorganic/organic ratio (see Table 3.6). To this end we used a block copolymer containing 10 wt.-% PDMAEMA and molecular weight of 107,200 g/mol (polymer A, see Table 3.1) and cast films (see Experimental Part and Table 3.6) with inorganic/organic ratios of 0.5, 1 and 2.5 (samples 1, 2 and 3, respectively). Hybrids with inorganic/organic weight ratios as high as 4 (and probably even higher) can be synthesized without macrophase separation between PUMVS and PI-*b*-PDMAEMA. Favorable enthalpic interactions, e.g., hydrogen bonds between the PUMVS and PDMAEMA, are most likely responsible for this high tolerance similar to what is observed in block copolymer – aluminosilicate systems [34].

Table 3.6. Characterization of PI-*b*-PDMAEMA/ PUMVS hybrids

Sample	MW PI-*b*-PDMAEMA (g/mol)	Weight fraction PDMAEMA (wt.-%)	PUMVS/ PI-*b*-PDMAEMA weight ratio	d spacing (nm)	Morphology
1	107k	10	0.5	53.7	hexagonal cylinder
2	107k	10	1	55.1	lamellar
3	107k	10	2.5	61.6	inverse hexagonal cylinder
4	31k	33	2	28.6	inverse hexagonal cylinder
5	31k	33	2	17.5	inverse hexagonal cylinder

Hybrid structure was investigated by small angle x-ray scattering (SAXS). SAXS traces of samples 1 and 3 (Figure 3.6a) both show at least two higher order reflections at angular positions of $\sqrt{3}$ and $\sqrt{4}$ of the first-order maximum, consistent with cylinders packed in a hexagonal lattice, whereas sample 2 shows at least two higher order reflections at angular position of 2 and 3 of the first-order maximum, consistent with a lamellar morphology. Transmission electron microscopy (TEM) was performed to corroborate these assignments. Representative bright-field TEM images of the three composites are shown in Figure 3.7a-c. The contrast arises from the density difference between PI and PDMAEMA/PUMVS domains, the latter appearing darker. Figure 3.7a (sample 1) clearly suggests the hexagonal packing of dark cylinders in a light matrix, which translates to PDMAEMA/PUMVS cylinders in a PI matrix. Figure 3.7b (sample 2) shows alternating layers of light (PI) and dark (PDMAEMA/PUMVS) lamellar domains. Finally, Figure 3.7c (sample 3) suggests the

reverse of the situation in Figure 3.7a, i.e., hexagonally arranged light (PI) cylinders in a dark (PDMAEMA/PUMVS) matrix. The TEM observations are thus consistent with the interpretation of the SAXS results.

The sequence of observed morphologies upon mixing of PUMVS into PI-*b*-PDMAEMA strongly suggests that there is preferential swelling of the PDMAEMA domains of the block copolymer by the PUMVS thus leading to phase transitions at higher loadings. For a system without additional favorable enthalpic interactions one would expect, however, that upon subsequent crosslinking of the PUMVS it would segregate from the PDMAEMA. The morphology control demonstrated here suggests that if phase separation occurs, it may be freezing in at early stages thus preventing macroscopic segregation similar to what is observed in block-copolymer epoxy-resin mixtures [22, 23]. To what extent or if at all segregation occurs on the local molecular level in the present systems remains an open question, however. In this context it is interesting to calculate effective volume fractions taking PI as one block and PDMAEMA/PUMVS as the other block in order to compare the results to known block copolymer morphology diagrams. The calculation is based on the original volume fractions of the PI-*b*-PDMAEMA block copolymer, the inorganic/organic ratio and the densities of PI, PDMAEMA and PUMVS (0.9, 1.1 and 1.1 g/cm^3 respectively) [24, 35]. The resulting volume fractions of 0.65, 0.50 and 0.30 showing hexagonal, lamellar and hexagonal morphologies for sample 1, 2 and 3, respectively, are consistent with expected morphologies from, e.g., mean-field calculations of block copolymers [36, 37].

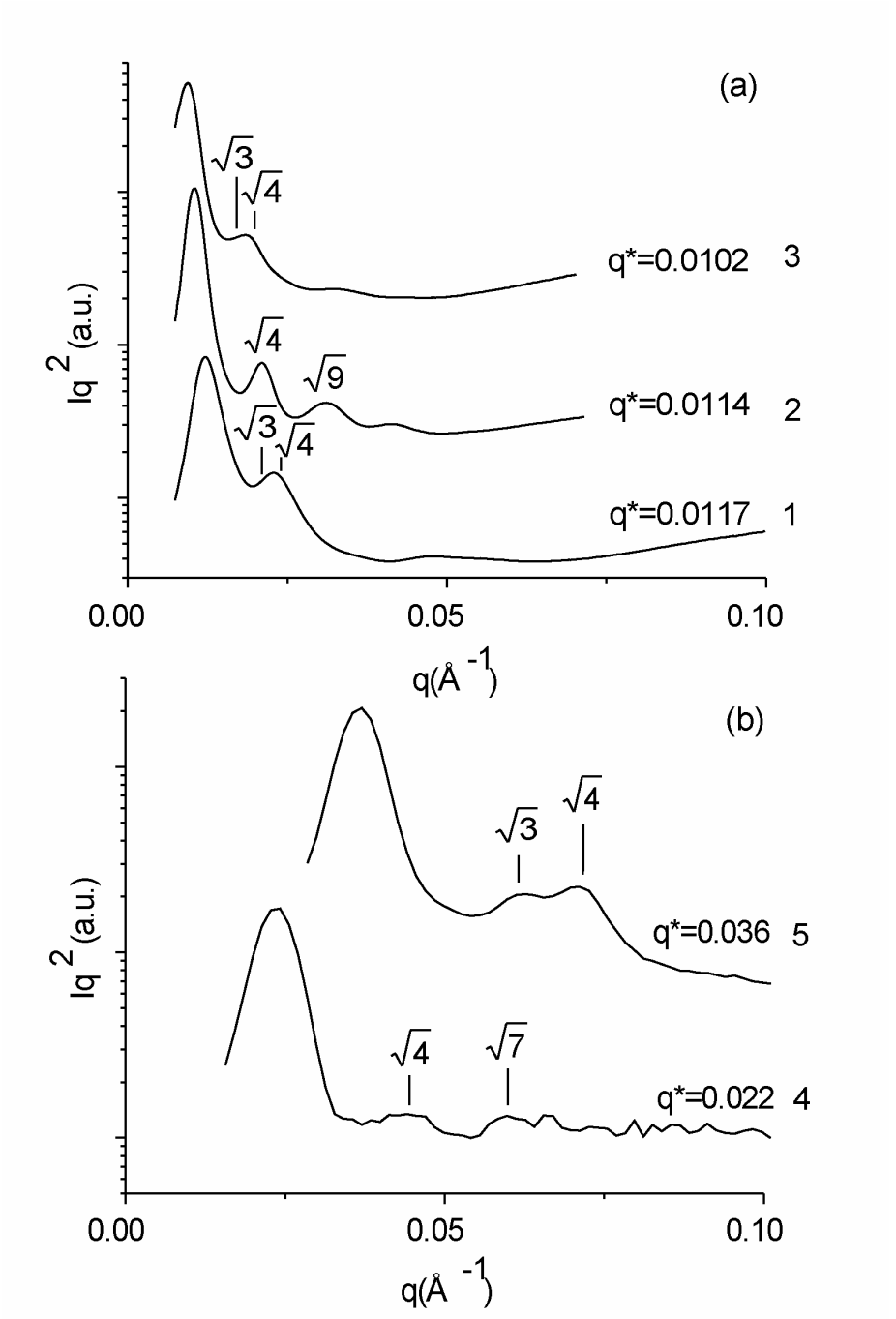

Figure 3.6. (a) SAXS traces of different morphologies of as-made composites by adding different amounts of inorganic to one polymer (polymer A in Table 3.1); 1. hexagonal cylinder morphology, 2. lamellar morphology and 3. hexagonal cylinder morphology. (b) SAXS traces for the as-made composite (4) and the resulting ceramic after calcinations to 1500 ºC (polymer C in Table 3.1) (5).

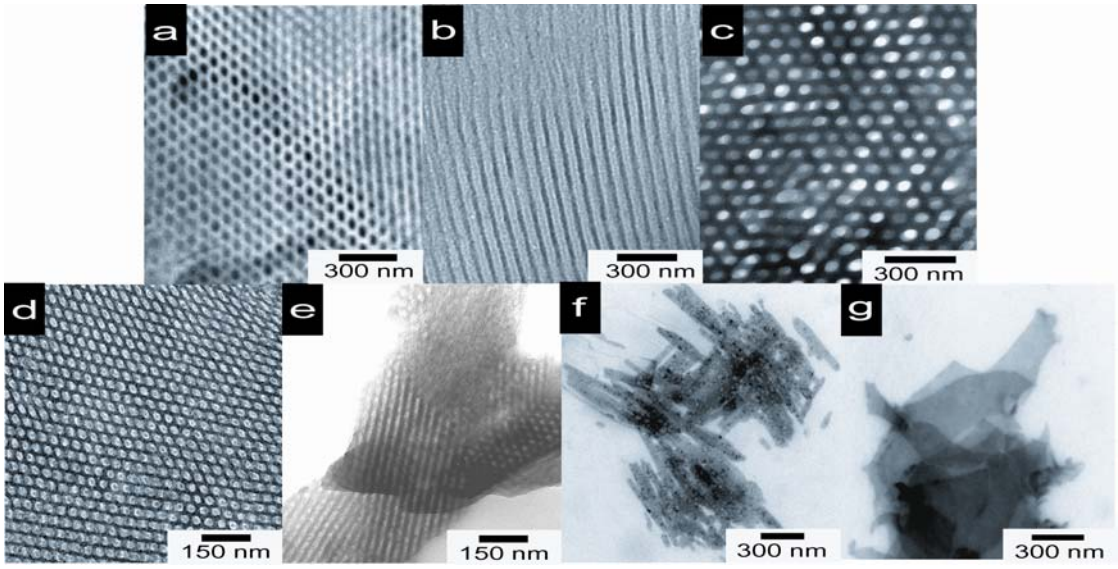

Figure 3.7. Bright-field TEM images (a-c) revealing different morphologies of as-made composites obtained by adding different amounts of inorganic to one polymer; images are consistent with (a) hexagonal cylinder morphology (sample 1), (b) lamellar morphology (sample 2) and (c) inverse hexagonal cylinder morphology (sample 3). Bright-field TEM images for an as-made composite (sample 4) (d) and the resulting ceramic after calcinations to 1500 ºC (sample 5) (e), demonstrating that the hexagonal structure is preserved during heat treatment. Bright-field TEM images of individual nanoparticles after dissolution of hybrids with hexagonal (sample 1 dissolved) (f) and lamellar (sample 2 dissolved) (g) morphologies.

The lattice (d)-spacing, and thereby the size of the domains, can be tuned by varying the molecular weight and composition of the parent block copolymer as well as by hybrid composition (see Table 3.6). Hybrid sample 4 was synthesized using a block copolymer containing 33 wt.-% PDMAEMA with a molecular weight of 31 000 g/mol (polymer C in Table 3.1), i.e., much smaller than the 107 200 g/mol polymer used to synthesize samples 1 to 3. The SAXS diffractogram of hybrid sample 4, derived from this polymer with an inorganic/organic ratio of 2, is depicted in Figure 3.6b. The SAXS trace shows at least two higher order reflections at angular positions of $\sqrt{3}$ and $\sqrt{4}$ of the first-order maximum, consistent with cylinders packed in a hexagonal lattice. Comparison of the traces of samples 3 and 4, both exhibiting a

hexagonal structure, reveals a significant shift in lattice-spacing from 53.7 nm to 28.6 nm, respectively, indicating the tunability of the domain size.

Composites rich in PI, i.e., with hexagonal and lamellar morphology, can be dissolved in an organic solvent for PI (e.g., in toluene or THF) leading to nanoparticles (nanoobjects) with well defined size and shape, as demonstrated earlier for block copolymer-aluminosilicate composites [38]. To this end, sample 1 and 2 with hexagonal and lamellar morphology, respectively, were dissolved in THF and the resulting nanoparticles were imaged with TEM. The images in Figures 3.7f and g qualitatively demonstrate that this concept works. Furthermore, such nanoparticles could, in a subsequent step, be transformed to non-oxide-type ceramics through temperature processing, preserving their shape [38]. Alternatively, composites with an inverse hexagonal structure (i.e. a crosslinked PUMVS matrix) can be used to prepare mesoporous solids [15]. To this end, sample 4 was calcined to 1500 °C under Ar/H_2 (see Experimental Part) to remove the organic material and convert the PUMVS into a mesoporous ceramic material (sample 5). The SAXS diffractogram of sample 5 reveals two higher order reflections at angular positions of $\sqrt{3}$ and $\sqrt{4}$ of the first-order maximum (see Figure 3.6b), suggesting that the hexagonal lattice is indeed preserved. All reflections of sample 5 are shifted to higher q-values compared to the composite (sample 4), however, indicating that, as expected, the sample shrinks upon calcination. The corresponding reduction in characteristic lattice spacing upon heating to 1500 °C from 28.6 to 17.5 nm with 39% is very similar to what is observed for aluminosilicate hybrids calcined to 550 °C [39]. TEM images of both samples 4 and 5 (Figures 3.7d and e) corroborated the hexagonal structures of composite and ceramic materials, respectively, demonstrating that the hexagonal structure is preserved upon heating to 1500 °C into a mesoporous ceramic material. The composition of such

ceramic materials has been described in reference 15 and representative values are shown in Table 3.3.

Conclusion

In the present study we showed that the amphiphilic block copolymer PI-*b*-PDMAEMA can be used as a structure directing agent for PUMVS, a precursor for high temperature non-oxide ceramics. In studies of hybrid composition as a function of synthesis conditions we demonstrated that PUMVS is very susceptible to reaction with water, upon which the chemical composition of hybrid material is changed from mainly Si-H-C-N to predominantly Si-H-C-O. Data suggest that this transformation is particularly important for materials with high surface-to-volume ratio. Solid state NMR and RBS data revealed that preparation and storage under dry conditions prevented reaction with water, preserving the original chemical composition. In studies on hybrid morphology we showed that by systematically increasing the inorganic/organic ratio a sequence of morphologies can be obtained from a single block copolymer, as expected from typical block copolymer phase diagrams. By changing the molecular weight of the block copolymer the lattice constants/domain sizes can be tuned. Dissolution of hexagonal/lamellar hybrids rich in PI can lead to nanoparticles of well defined shape and size. High temperature treatment up to 1500°C of inverse hexagonal composites rich in crosslinked PUMVS resulted in a ceramic that retained the morphology of the parent hybrid composite. The present block copolymer directed co-assembly (bottom-up) approach thus provides a versatile method to synthesize mesostructured high temperature non-oxide-type ceramics with tunable morphology and domain size, which may lead to materials with interesting mechanical, thermal and chemical properties.

Acknowledgements

The financial support of the National Science foundation (awards DMR-0605856 and DMR-NIRT-0404195) is gratefully acknowledged. The work was further supported by the Cornell Center for Materials Research (CCMR), a Materials Research Science and Engineering Center of the National Science Foundation (DMR-0520404). X-ray diffraction at the Cornell High Energy Synchrotron Source (CHESS) is supported by the National Science Foundation under award DMR-0225180. Solid state NMR facilities were supported by the Canadian Foundation for Innovation.

REFERENCES

[1] C. T. Kresge, M. E. Leonowicz, W. J. Roth, J. C. Vartuli, J. S. Beck, *Nature* **1992**, *359*, 710.

[2] M. Templin, A. Franck, A. DuChesne, H. Leist, Y. M. Zhang, R. Ulrich, V. Schadler, U. Wiesner, *Science* **1997**, *278*, 1795.

[3] D. Y. Zhao, J. L. Feng, Q. S. Huo, N. Melosh, G. H. Fredrickson, B. F. Chmelka, G. D. Stucky, *Science* **1998**, *279*, 548.

[4] P. D. Yang, D. Y. Zhao, D. I. Margolese, B. F. Chmelka, G. D. Stucky, *Nature* **1998**, *396*, 152.

[5] M. Kamperman, U. Wiesner, in *Block Copolymers in Nanoscience* (Eds.: M. Lazzari, G. Liu, S. Lecommandoux), Wiley-VCH, Weinheim, **2006**.

[6] Y. L. Li, E. Kroke, R. Riedel, C. Fasel, C. Gervais, F. Babonneau, *Applied Organometallic Chemistry* **2001**, *15*, 820.

[7] S. R. Shah, R. Raj, *Acta Materialia* **2002**, *50*, 4093.

[8] R. Raj, R. Riedel, G. D. Soraru, *Journal of the American Ceramic Society* **2001**, *84*, 2158.

[9] D. Seyferth, C. Strohmann, N. R. Dando, A. J. Perrotta, *Chemistry of Materials* **1995**, *7*, 2058.

[10] J. M. Schwark, *Polymer Preprints* **1991**, *32*, 567.

[11] S. Yajima, J. Hayashi, M. Omori, *Chemistry Letters* **1975**, 931.

[12] Y. F. Shi, Y. Meng, D. H. Chen, S. J. Cheng, P. Chen, H. F. Yang, D. Y. Zhao, *Advanced Functional Materials* **2006**, *16*, 561.

[13] I. K. Sung, Christian, M. Mitchell, D. P. Kim, P. J. A. Kenis, *Advanced Functional Materials* **2005**, *15*, 1336.

[14] C. B. W. Garcia, C. Lovell, C. Curry, M. Faught, Y. M. Zhang, U. Wiesner, *Journal of Polymer Science Part B-Polymer Physics* **2003**, *41*, 3346.

[15] M. Kamperman, C. B. W. Garcia, P. Du, H. S. Ow, U. Wiesner, *Journal of the American Chemical Society* **2004**, *126*, 14708.

[16] J. L. Wan, A. Alizadeh, S. T. Taylor, P. R. L. Malenfant, M. Manoharan, S. M. Loureiro, *Chemistry of Materials* **2005**, *17*, 5613.
[17] J. Wan, P. R. L. Malenfant, S. T. Taylor, S. M. Loureiro, M. Manoharan, *Materials Science and Engineering A* **2007**, *463*, 78.

[18] P. R. L. Malenfant, J. Wan, S. T. Taylor, M. Manoharan, *Nature Nanotechnology* **2007**, *2*, 43.

[19] S. Renker, Max Planck Institute for Polymer Research (Mainz, Germany), **2003**.

[20] S. Creutz, P. Teyssie, R. Jerome, *Macromolecules* **1997**, *30*, 6.

[21] B. M. Fung, A. K. Khitrin, K. Ermolaev, *Journal of Magnetic Resonance* **2000**, *142*, 97.

[22] M. A. Hillmyer, P. M. Lipic, D. A. Hajduk, K. Almdal, F. S. Bates, *Journal of the American Chemical Society* **1997**, *119*, 2749.

[23] P. M. Lipic, F. S. Bates, M. A. Hillmyer, *Journal of the American Chemical Society* **1998**, *120*, 8963.

[24] CERASET SN Inorganic Polymer Technical Bulletin. Lanxide Company, 1997.

[25] Information about RUMP can be obtained at the following URL:

http://www.genplot.com/.

[26] M. Birot, J. P. Pillot, J. Dunogues, *Chemical Reviews* **1995**, *95*, 1443.

[27] W. R. Schmidt, L. V. Interrante, R. H. Doremus, T. K. Trout, P. S. Marchetti, G. E. Maciel, *Chemistry of Materials* **1991**, *3*, 257.

[28] H. Brequel, J. Parmentier, S. Walter, R. Badheka, G. Trimmel, S. Masse, J. Latournerie, P. Dempsey, C. Turquat, A. Desmartin-Chomel, L. Le Neindre-Prum, U. A. Jayasooriya, D. Hourlier, H. J. Kleebe, G. D. Soraru, S. Enzo, F. Babonneau, *Chemistry of Materials* **2004**, *16*, 2585.

[29] W. Toury, F. Babonneau, *Journal of the European Ceramic Society* **2005**, *25*, 265.

[30] J. K. D. MacKenzie, Smith, M.E., *Multinuclear Solid-State NMR of Inorganic Materials*, Pergamon Materials Series, **2002**.

[31] M. Camail, H. Essaoudi, A. Margaillan, J. L. Vernet, *European Polymer Journal* **1995**, *31*, 1119.

[32] J. W. Cook, S. Edge, D. E. Packham, A. S. Thompson, *Journal of Applied Polymer Science* **1997**, *65*, 1379.

[33] M. Zemanova, E. Lecomte, P. Sajgalik, R. Riedel, *Journal of the European Ceramic Society* **2002**, *22*, 2963.

[34] S. C. Warren, F. J. Disalvo, U. Wiesner, *Nature Materials* **2007**, *6*, 156.

[35] J. Brandrop, E. H. Immergut, *Polymer Handbook*, Wiley, New York, **1975**.

[36] M. W. Matsen, F. S. Bates, *Macromolecules* **1996**, *29*, 7641.

[37] A. K. Khandpur, S. Forster, F. S. Bates, I. W. Hamley, A. J. Ryan, W. Bras, K. Almdal, K. Mortensen, *Macromolecules* **1995**, *28*, 8796.

[38] R. Ulrich, A. Du Chesne, M. Templin, U. Wiesner, *Advanced Materials* **1999**, *11*, 141.

[39] A. C. Finnefrock, R. Ulrich, G. E. S. Toombes, S. M. Gruner, U. Wiesner, *Journal of the American Chemical Society* **2003**, *125*, 13084.

CHAPTER 4

MORPHOLOGY CONTROL IN BLOCK COPOLYMER/ POLYMER DERIVED CERAMIC PRECURSOR NANOCOMPOSITES[3]

Abstract

Block copolymer – polymer derived ceramic (PDC) precursor nanocomposites were prepared using amorphous poly(isoprene–*block*–dimethylaminoethyl methacrylate) (PI–*b*–PDMAEMA) and semicrystalline poly(isoprene–*block*–ethylene oxide) (PI–*b*–PEO) block copolymers as structure directing agents for poly(ureamethylvinyl)silazane (PUMVS). Studies on hybrid morphologies were performed using Small Angle X-ray Scattering (SAXS) and Transmission Electron Microscopy (TEM). In the amorphous system, the PUMVS preferentially swells the PDMAEMA and a systematic increase of the PUMVS to PI-*b*-PDMAEMA weight ratio resulted in lamellar, hexagonally packed cylindrical and body-centered cubic packed spherical morphologies. Crystallization of PEO in PI-*b*-PEO/PUMVS hybrids led to crystalline lamellar morphologies over a large range of PUMVS to PI-*b*-PEO weight ratios. The d-spacing of the PI-b-PEO/ PUMVS hybrids increased only slightly upon PUMVS loading, because the strong chain stretching in the PI block is progressively relaxed as the PUMVS swells the PEO. Annealing of the PI-*b*-PEO/PUMVS system at elevated temperatures led to suppression of the PEO crystallization, resulting in order-order phase transitions.

[3] Kamperman, M.; Fierke, M. A.; Garcia, C. B. W.; Wiesner, U.: submitted.

Introduction

A convenient and effective way to construct well-defined polymer – inorganic nanostructured composite materials is to use block copolymers as structure directing agents. The prevalent route to preparing such hybrid materials is using sol-gel chemistry where a solution containing inorganic precursors and the block copolymer co-assemble to form a spectrum of mesophases [1-3]. In these systems the final morphology of the composite is not dictated by free energy considerations only, but also depends on the kinetics of gel formation.

Mixing a low molecular weight thermosetting resin with a block copolymer was shown to be a successful method for the preparation of all-organic nanostructured hybrid materials [4-6]. The low molecular weight resin selectively swells one of the blocks. Well-defined mesophases were observed by systematically increasing the resin to block copolymer volume fraction. Self-assembly was induced by solvent evaporation and was independent from polymerization of the resin, thereby avoiding the kinetic limitations of sol-gel approaches. More recently, we showed that this method can be applied to mixtures of an amphiphilic block copolymer with polymer derived ceramic (PDC) precursors, providing a one-pot-type pathway towards mesoporous high temperature ceramics [7,8]. In the meantime, similar results have been produced with different structure directing agents [9,10] and the approach has been extended towards organosilicate thin films [11].

This paper explores in more detail the underlying factors controlling morphology of block copolymer – PDC precursor derived hybrid materials. To this end, we investigated morphological differences resulting from the use of either a semicrystalline or an amorphous diblock copolymer as structure directing agents. Poly(isoprene–*block*–ethylene oxide) (PI–*b*–PEO) and poly(isoprene–*block*–dimethylaminoethyl methacrylate) (PI–*b*–PDMAEMA), were used as semicrystalline

and amorphous polymers, respectively, both systems being amphiphilic. The PDC precursor was a poly(ureamethylvinyl)silazane (PUMVS), the structure of which is shown in Figure 4.1 together with the molecular structures of the block copolymers.

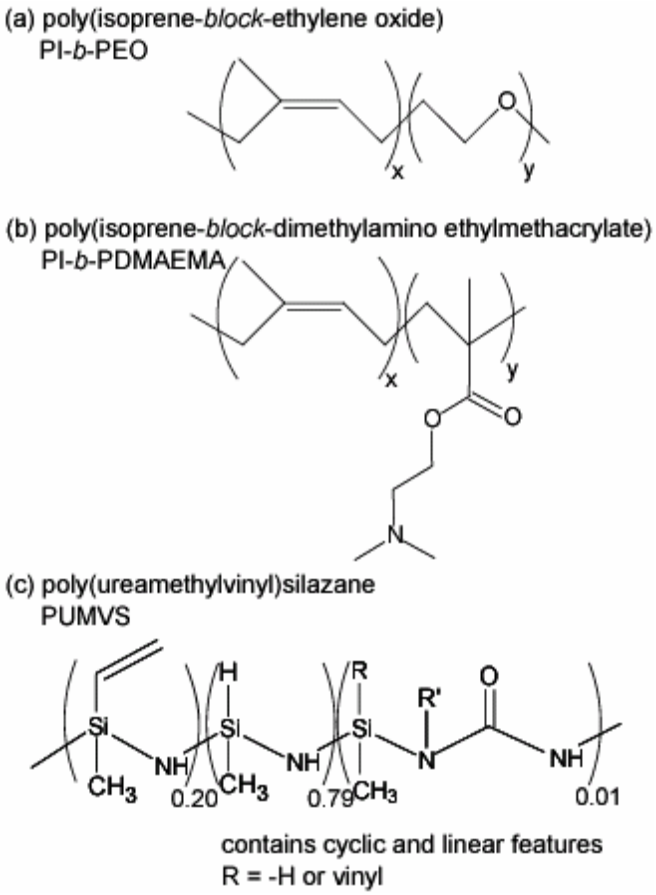

Figure 4.1. Chemical structures of (a) poly(isoprene–*block*–ethylene oxide), (b) poly(isoprene–*block*–dimethylaminoethyl methacrylate) and (c) poly(ureamethylvinyl)silazane (PUMVS). No information is available about the nature of R'.

Blending PUMVS with either the semicrystalline or the amorphous block copolymer is expected to lead to preferential swelling of their hydrophilic domains, i.e. PEO or PDMAEMA (see Figure 4.1), thereby increasing the effective hydrophilic volume fraction. The hybrid material was solidified by crosslinking the PUMVS with a radical initiator. We show below that the PUMVS does not suppress the

crystallization of the PEO in the hybrid materials resulting in crystalline lamellar morphologies over a wide range of compositions. We further demonstrate that this crystallinity can be suppressed upon annealing of the hybrids at elevated temperatures resulting in a mesophase evolution similar to that in the amorphous block copolymer/PUMVS hybrids, induced by systematically increasing the PUMVS to block copolymer weight fraction. Morphological changes and structural details upon swelling of the hydrophilic block by PUMVS are investigated with Small Angle X-ray Scattering (SAXS) and Transmission Electron Microscopy (TEM).

Experimental Section

Materials and Instrumentation

Materials. For the block copolymer synthesis *sec*-butyllithium (1.4 M in cyclohexane, Aldrich), potassium (98%, Fluka) and naphthalene (99%, Sigma-Aldrich) were used as received. Isoprene (99%, Aldrich), ethylene oxide (99.5+%, Aldrich), cyclohexane (99%, J. T. Baker), tetrahydrofuran (THF) (99%, J. T. Baker) and 1,1-diphenylethylene (97%, Aldrich) were distilled from *n*-butyllithium (1.6 M in hexanes, Sigma-Aldrich) prior to use. The monomer dimethylaminoethyl methacrylate (DMAEMA) (98%, Aldrich) was stirred over CaH_2 (90-95%, Aldrich) and distilled under vacuum. Methanolic HCl (3 N, Supelco) was freeze-pump-thawed three times prior to use.

For the hybrid synthesis tetrahydrofuran (99%, J. T. Baker), toluene (99.5+%, J. T. Baker), the ceramic precursor, Ceraset (KiON Corp.) and the radical initiator, dicumyl peroxide (Aldrich) were used as received.

Instrumentation

Gel Permeation Chromatography (GPC). Measurements were performed in 98% tetrahydrofuran (THF) and 2% N,N-dimethylacetamide at room temperature using 5 μm Waters Styragel columns (10^3, 10^4, 10^5, 10^6 Å, 30 cm each; Waters Corporation, Milford, MA) at a flow rate of 1.0 mL/min. A Waters 490 programmable multi-wavelength UV diode array detector (operated at λ = 260 nm) and a Waters 410 RI detector operated at 25 °C were used. Raw data were processed using PSS-Win GPC V6.2 software (Polymer Standards Service, Mainz, Germany). Molecular weights (M_w) and M_w – distributions (M_w/M_n) were calculated using a polyisoprene calibration curve.

^{1}H Nuclear Magnetic Resonance (NMR). ^{1}H solution NMR spectra were recorded on a Varian INOVA 400 MHz spectrometer using $CDCl_3$ signal (δ = 7.27 ppm) as an internal standard.

Small Angle X-Ray Scattering (SAXS). Experiments were performed at the Cornell High Energy Synchrotron Source (CHESS). Data were collected with a CCD 2-D detector operating at X-ray energy corresponding to 1.223 Å, sample-to-detector distance of 165.0 cm and exposure times of 1-20 sec.

Transmission Electron Microscopy (TEM). Samples were ultrathin sectioned with a Leica Ultracut UCT microtome at -60 ºC. Sample slices were collected on a water/DMSO eutectic solution and transferred to 300 mesh copper grids (no carbon film was used). TEM was performed on a Tecnai T12 at 120 kV.

Differential scanning calorimetry (DSC) was performed on hybrids with a Thermal Advantage DSC Q100 (TA Instruments, Inc.), calibrated with an indium standard. Before taking measurements, samples were heated to 80 ºC, then cooled to -20 ºC and annealed for 1 h at -20 ºC. Measurements were taken on heating from -20 to 80 ºC at 5 ºC/min.

Synthesis

Block copolymer synthesis. The general synthetic procedures of the synthesis of poly(isoprene-*block*-ethylene oxide) (PI-*b*-PEO) and poly(isoprene-*block*-dimethylaminoethyl methacrylate) (PI-*b*-PDMAEMA) have been previously reported [12-14]. A slightly modified synthesis was used here and is summarized in Figure 4.2. Polymers were synthesized by anionic polymerization under anhydrous and air-free conditions using a glovebox and Schlenk line techniques.

PI-*b*-PEO. Sec-butyl lithium was used to initiate isoprene in cyclohexane. After 8 hours of polymerization at room temperature, the polyisoprene was end-capped with ethylene oxide and stirred overnight (caution: ethylene oxide is a toxic gas at room temperature!). Polymerization was terminated with methanolic HCl. Cyclohexane was removed by rotary evaporation, and the polymer was washed three times with water in chloroform (50/50 vol%). Chloroform was removed by rotary evaporation and the polymer was dried for 24 hours at 65 °C in a vacuum oven. GPC was used to determine the molecular weight of PI. An amount of KCl was added that was five times the number of moles of PI chains. The sample was dried for two more days at 65 °C in a vacuum oven. Anhydrous THF (distilled first from potassium, then n-butyl lithium) was added to the PI to dissolve it. The solution was titrated with potassium napthalide (~1.0 M in THF) until a green color persisted. Ethylene oxide was then added to the PI solution and the PEO was allowed to polymerize for five days. Polymerization was terminated with methanolic HCl. Solvent was removed by rotary evaporation and the polymer was washed three times with water in chloroform (50/50 vol%). Chloroform was removed by rotary evaporation and the polymer was placed in a vacuum oven for three days at 65 °C to remove naphthalene and residual water.

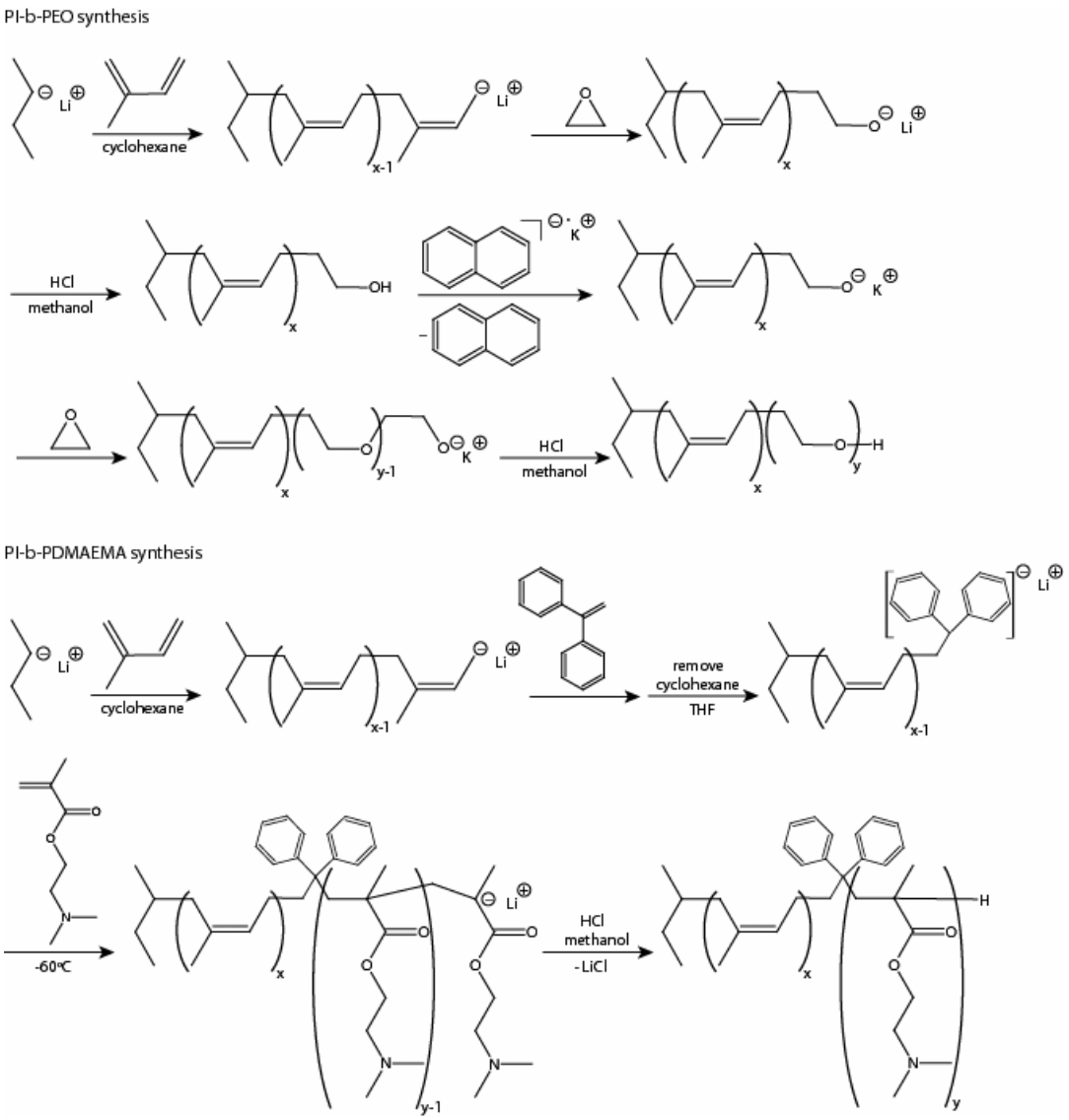

Figure 4.2. Synthesis of PI-*b*-PEO and PI-*b*-PDMAEMA.

PI-*b*-PDMAEMA. Sec-butyl lithium was used to initiate isoprene in cyclohexane. After 8 hours of polymerization at room temperature, cyclohexane was removed on a vacuum line and anhydrous THF was subsequently added to the PI in a glovebox. A small amount of the PI was removed via syringe, terminated with methanolic HCl, and subjected to GPC to determine the PI MW. Polyisoprene was end-capped with a 5-fold excess of diphenylethylene and stirred for 30 min. The polymer solution was cooled to -60 °C before the addition of DMAEMA.

Polymerization was allowed to proceed for several hours before the reaction was terminated with methanolic HCl. To purify the polymer, it was precipitated in cold methanol and dried on a vacuum line for several days.

The polymers were characterized by GPC to give the final polydispersity. ^{1}H NMR was used to determine the chemical composition of the block copolymer. The resulting polymers had number average molecular weights in the range of 20 – 107 kg·mol^{-1}, 67 – 90 wt.-% PI and a polydispersity below 1.2, see Table 4.1.

Table 4.1. Characterization of block copolymers

	Block copolymer	**MW (g/mol)**	**polydispersity**	**wt.-% PI**
A	PI-*b*-PDMAEMA	107 200	1.03	90
B	PI-*b*-PDMAEMA	24 300	1.06	85
C	PI-*b*-PDMAEMA	29 000	1.04	83
D	PI-*b*-PDMAEMA	84 000	1.07	79
E	PI-*b*-PDMAEMA	31 100	1.05	67
F	PI-*b*-PEO	22 100	1.05	85

Hybrid Preparation. Synthesis of mesostructured hybrids was performed by a one-pot synthesis approach, in which the ceramic precursor is expected to swell the hydrophilic block. Films were cast beneath a hemispherical dish made from the bottom half of a 1-L flask. Heating was controlled using a IKA RET control visc IKAMAG digital hotplate. The chemical structures of the block copolymers and the PUMVS are shown in Figure 4.1. In a typical synthesis a 5 wt.-% block copolymer solution in THF or toluene was mixed with the ceramic precursor and the radical initiator dicumyl peroxide (1 wt.-% with respect to the mass of PUMVS) and stirred for 1h. The solution was subsequently poured into a Teflon Petri dish and a film cast by solvent evaporation on a hotplate at 50 ºC followed by annealing for 24 h under

vacuum at 50 ºC. This resulted in a film thickness of about 500 μm. The temperature was then increased to 130 ºC for 3 h to crosslink the PUMVS.

Results and Discussion

1. Morphology diagram for PI-*b*-PDMAEMA/ PUMVS hybrids

The presence of a semicrystalline block in a block copolymer adds an extra level of complexity to the morphological behavior as microphase separation can be driven by both block incompatibility and crystallization. In order to better understand the morphological differences resulting from using a semicrystalline block copolymer as a structure directing agent for PDC precursors it is insightful to compare the morphological behavior with hybrids from an amorphous block copolymer. To this end we used five different PI-*b*-PDMAEMA block copolymers with different PDMAEMA weight fractions (polymers A – E in Table 4.1) and cast 25 films with PUMVS/ block copolymer weight ratios ranging between 0.12 and 4.03 (see Experimental Part and Table 4.2). The resulting hybrid morphologies were determined by a combination of SAXS and TEM as described in references 8 and 15 (see also below). The behavior of the PI-*b*-PDMAEMA/PUMVS system is depicted in the form of a morphology diagram in Figure 4.3 and results are summarized in Table 4.2.

The morphology map is based on the weight fraction of each component (PI, PDMAEMA and PUMVS). In this diagram, from left to right, the five dark lines connect compositions derived from the five block copolymers by adding increasing amounts of the PDC precursor. Compositions showing the same hybrid morphology have been color coded. We found lamellar (L), hexagonally packed cylinder (C) and body-centered cubic packed spherical (S) hybrid morphologies. The map demonstrates that by systematically increasing the PUMVS/ block copolymer ratio multiple morphologies can be obtained from the same block copolymer. This is consistent with

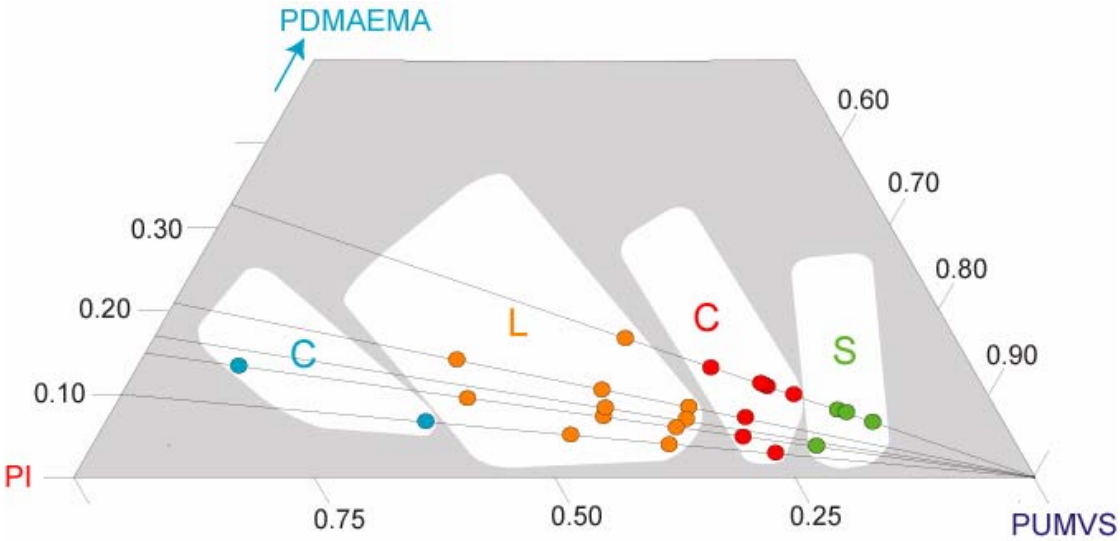

Figure 4.3. Morphology diagram mapping the morphologies for various weight fractions of the PI-*b*-PDMAEMA/PUMVS system. Compositions showing the same hybrid morphology are color coded and white domains suggest regions with well-defined hybrid morphologies: cylindrical (C) blue, lamellar (L) orange, cylindrical (C) red, and spherical (S) green. Dark lines connect compositions derived from a specific block copolymer by adding increasing amounts of PDC precursor.

Table 4.2. Compositions of PI-*b*-PDMAEMA/PUMVS hybrids

Composite	PUMVS/ PI-*b*-PDMAEMA weight ratio	Morphology*	Composite	PUMVS/ PI-*b*-PDMAEMA weight ratio	Morphology*
A-1	0.52	C	D-2	0.99	L
A-2	0.98	L	D-3	1.49	L
A-3	1.52	L	D-4	1.99	C
A-4	2.54	C	E-1	0.99	L
B-1	0.12	C	E-2	1.49	C
B-2	0.57	L	E-3	1.98	C
B-3	1.07	L	E-4	2.00	C
B-4	1.49	L	E-5	2.03	C
B-5	2.08	C	E-6	2.48	C
B-6	2.97	S	E-7	3.18	S
C-1	1.07	L	E-8	3.29	S
C-2	1.55	L	E-9	4.03	S
D-1	0.50	L			

* cylindrical (C), lamellar (L) and spherical (S)

earlier TEM and SAXS studies on this system [15]. The white areas in Figure 4.3 provide a rough guide which part of phase space the different morphologies cover.

2. Comparison of PI-*b*-PDMAEMA/ PUMVS with PI-*b*-PEO/ PUMVS hybrids

After exploring the PI-*b*-PDMAEMA/ PUMVS hybrid morphology space we subsequently compared the morphological behavior of two sets of hybrid samples, one derived from PI-*b*-PEO (polymer F in Table 4.1) and one from PI-*b*-PDMAEMA (polymer B in Table 4.1), i.e. from block copolymers with similar polymer characteristics. The polymers exhibited a hexagonally packed cylindrical morphology and d-spacings of 20.2 and 18.1 nm for PI-*b*-PEO and PI-*b*-PDMAEMA, respectively. Both sets of hybrids were prepared with very similar PUMVS/ block copolymer weight ratios and under identical conditions (see Table 4.3 and Experimental section). All of the cured samples were transparent, suggesting the lack of macroscopic phase separation between crosslinked PUMVS and block copolymer. TEM data corroborated this observation (see below). Macroscopic segregation may be prevented by mobility restrictions upon crosslinking and high free energy barriers to nucleation of block copolymer rich domains [5]. For the PI-*b*-PEO/PUMVS hybrids it is also very likely that the PUMVS is covalently bonded to the terminal hydroxy group of the PEO chain. Hydroxyl groups are known to react with PUMVS [9, 10, 15], creating a PUMVS network attached to the PEO chains, thereby preventing macroscopic segregation.

Table 4.3. Characterization of PI-*b*-PEO/ PUMVS and PI-*b*-PDMAEMA/ PUMVS hybrids

Sample	Block copolymer	PUMVS/block copolymer weight ratio	d-spacing (nm)	d-spacing increase (%)	Morphology
1	PI-*b*-PEO	0.12	24.6	-	C
2	PI-*b*-PEO	0.55	26.2	6.9	L
3	PI-*b*-PEO	1.05	27.3	10.6	L
4	PI-*b*-PEO	1.96	27.9	13.4	L
5	PI-*b*-PEO	2.50	29.7	20.7	L
6	PI-*b*-PDMAEMA	0.12	21.1	-	C
7	PI-*b*-PDMAEMA	0.57	23.4	10.9	L
8	PI-*b*-PDMAEMA	1.07	24.1	14.2	L
9	PI-*b*-PDMAEMA	2.08	27.7	31.3	C
10	PI-*b*-PDMAEMA	2.97	34.3	62.6	S
11	PI-*b*-PEO	2.30	29.6	-	L

2.1. Hybrid morphology

Hybrid structure was investigated by a combination of SAXS and TEM. Figure 4.4 shows, side by side, stack plots of SAXS traces of the different hybrids with compositions described in Table 3. Comparing scattering traces suggests that structure evolution as a function of weight % PUMVS is very different for the two hybrid systems. SAXS traces of all but one of the PI-*b*-PEO/PUMVS hybrids (Figure 4.4a) show at least one higher order reflection at angular position of $\sqrt{4}$ of the first-order maximum, consistent with a lamellar morphology. Only PI-*b*-PEO/PUMVS hybrid 1 with only 11 wt% PUMVS shows a higher order reflection at angular position $\sqrt{3}$ of the first-order maximum, consistent with cylinders packed in a hexagonal lattice. In contrast, SAXS traces of PI-*b*-PDMAEMA/PUMVS hybrids 6 and 9 (Figure 4.4b) both show a (broad) higher-order peak around angular positions of $\sqrt{3}$ and $\sqrt{4}$ of the

first-order maximum, consistent with cylinders packed in a hexagonal lattice; Hybrids 7 and 8 show at least one higher order reflection at angular position of $\sqrt{4}$ and $\sqrt{9}$ of the first-order maximum, respectively, both consistent with a lamellar morphology; Finally, sample 10 shows a (broad) higher order reflection around angular positions of $\sqrt{2}$ and $\sqrt{3}$ of the first-order maximum, consistent with a body-centered cubic packed spherical morphology. Thus, whereas the PI-*b*-PDMAEMA/PUMVS hybrid system shows a sequence of four morphologies upon increase of PUMVS content expected from e.g. mean-field calculations of block copolymers [16, 17], the structure evolution of the PI-*b*-PEO/ PUMVS systems seems to get stuck once the lamellar morphology is reached.

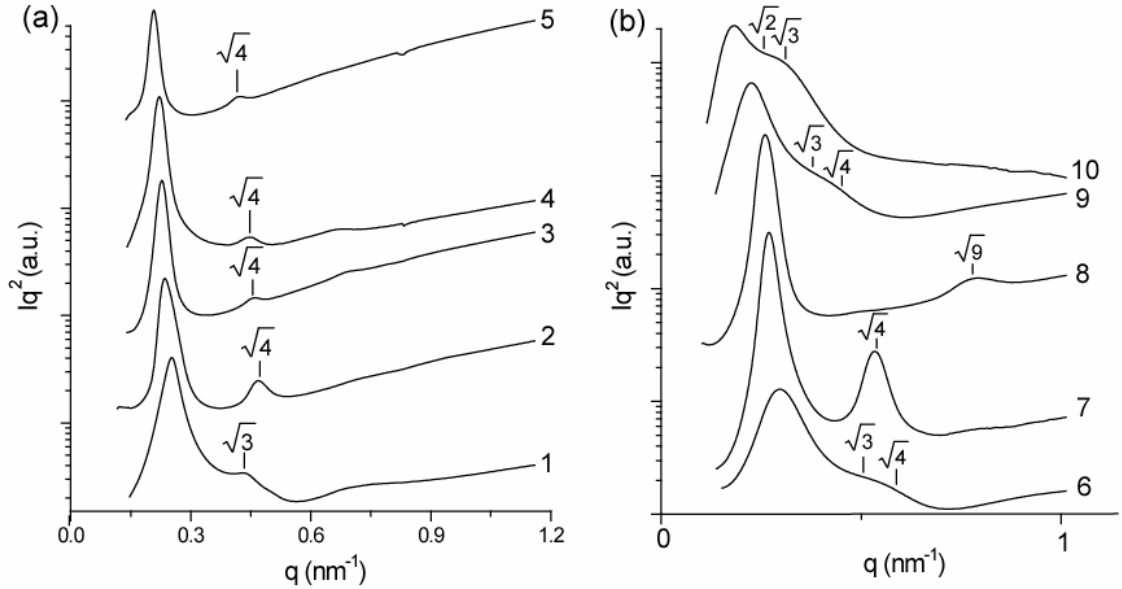

Figure 4.4. (a) SAXS traces of composite morphologies obtained by adding different amounts of PUMVS to same PI-*b*-PEO polymer (polymer F in Table 1). Data are consistent with 1: hexagonal cylinder morphology; 2-5: lamellar morphology. (b) SAXS traces of composite morphologies obtained by adding different amounts of PUMVS to the same PI-*b*-PDMAEMA polymer (polymer B in Table 1). Data are consistent with 6: hexagonal cylinder morphology; 7-8: lamellar morphology; 9: hexagonal cylinder morphology; 10: spherical morphology.

The latter behavior is similar to that of pure PI-*b*-PEO, where independent of composition at low temperatures (below ~50 °C), upon PEO crystallization, phases

revert to the crystalline lamellar morphology [18]. PI-*b*-PEO is an example of a strongly segregated system with soft confinement, with $T_{ODT} > T_c > T_g$, where T_{ODT} is the order-disorder transition (ODT) temperature, T_c is the crystallization temperature of the crystallizable block, and T_g is the glass-transition temperature of the amorphous block. The segregation strength between PI and PEO is sufficiently strong at molecular weights studied here to confine crystallization within spherical, cylindrical or lamellar domains. Therefore, PI-*b*-PEO with a PEO weight fraction between 0.17 – 0.30 will form a hexagonally packed cylindrical morphology with the PEO crystals confined in cylinders, whereas polymers with PEO weight fractions larger than ~0.30 will all form the crystalline lamellar morphology. The SAXS data of the PI-*b*-PEO/ PUMVS hybrids follow this trend, suggesting that PEO crystallizes even in the presence of crosslinked PUMVS. In order to support this hypothesis we performed Differential Scanning Calorimetry (DSC) measurements, see Figure 4.5.

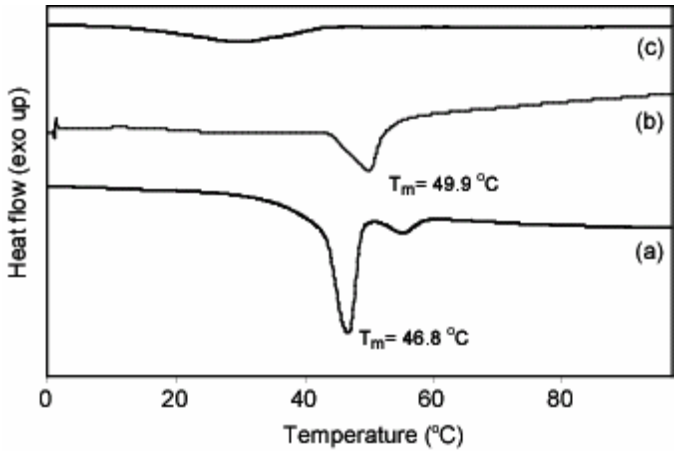

Figure 4.5. DSC heating curves (5 °C/min) of (a) PI-*b*-PEO block copolymer, (b) as-synthesized PI-*b*-PEO/PUMVS hybrid 2 and (c) PI-*b*-PEO/PUMVS hybrid 11 annealed at 300 °C.

Indeed, DSC curves of the pure PI-*b*-PEO block copolymer (Fig. 4.5a) and of the PI-*b*-PEO/PUMVS hybrid 2 (Fig. 4.5b) both show an endothermic peak upon heating associated with the melting of crystalline PEO. The double melting peak of

PEO in the pure polymer (Fig. 4.5a) is probably due to recrystallization during heating [19, 20].

2.2. Lattice spacing

Further inspection of the two series of SAXS traces in Figure 4.4 reveals a difference in the relative shifts of first-order maxima and corresponding d-spacings upon addition of PUMVS. Whereas the first order maxima of the PI-*b*-PDMAEMA/PUMVS system significantly moves to smaller q values upon increasing PUMVS content, those of the PI-*b*-PEO/PUMVS system only decrease slightly. Table 4.3 summarizes this result in the form of the respective lattice d-spacings. In order to rationalize this behavior one has to separate the influence of the PUMVS on the PI and PEO domains, respectively. To this end, TEM was performed on lamellar hybrids 2-4 to determine the thickness ratio of the PI and PEO/PUMVS domains. Representative bright-field TEM images of PI-*b*-PEO/ PUMVS hybrids 2, 3 and 4 are depicted in Figure 4.6a, b and c, respectively. The images show alternating layers of light (PI) and dark (PEO/PUMVS) lamellar domains, the contrast arising from the electron density difference between the domains. Closer inspection of these images reveals that with increasing PUMVS content the thickness of the PI domains decreases while that of the PEO/ PUMVS domains increases. This is corroborated by a more quantitative analysis of the SAXS data of Figure 4.4.

The individual layer thicknesses can be calculated from these SAXS data using:

$$l_{PEO/PUMVS} = \Phi_{PEO/PUMVS} L \quad (4.1)$$

$$l_{PI} = L - l_{PEO/PUMVS} = (1 - \Phi_{PEO/PUMVS}) L \quad (4.2)$$

where $\Phi_{PEO/PUMVS}$ is the effective PEO/PUMVS volume fraction and L the d-spacing provided by SAXS. The effective volume fractions are calculated based on the original

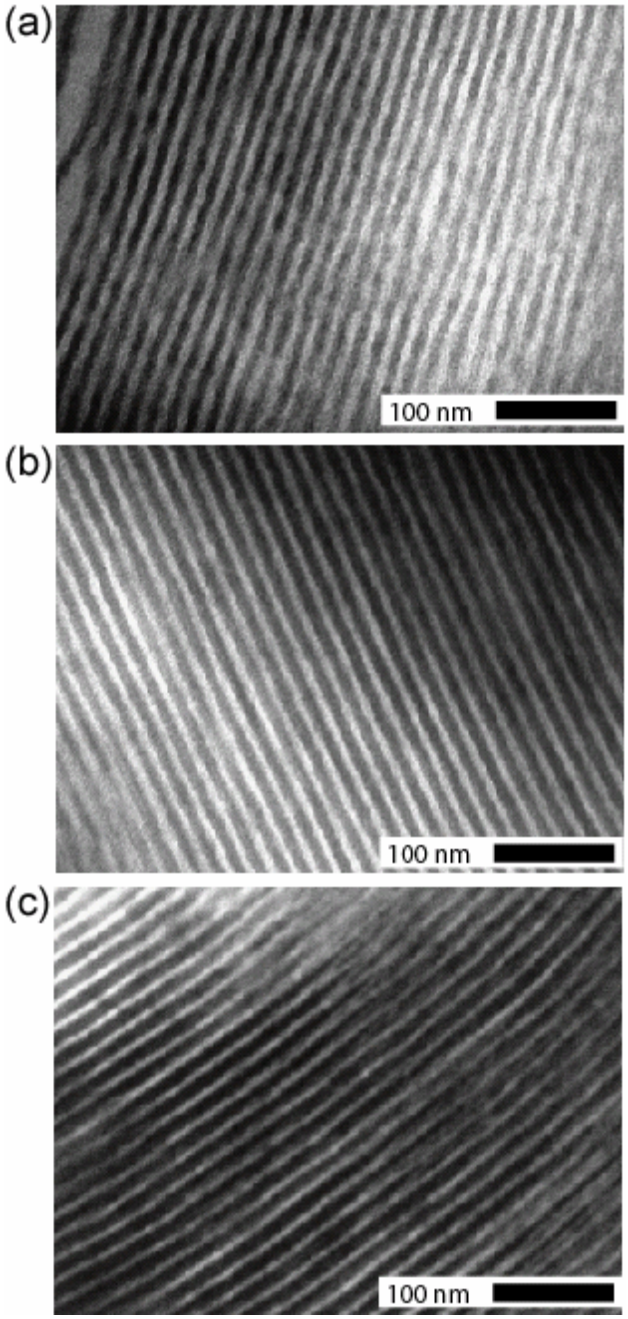

Figure 4.6. Bright-field TEM images revealing a lamellar morphology for hybrids 2 (a), 3 (b) and 4 (c).

volume fractions of the PI-*b*-PEO block copolymer, the PUMVS/ block copolymer ratio and the densities of PI, PEO and PUMVS (0.91, 1.12 and 1.12 g/cm^3), respectively [21, 22]. Results are given in Table 4.4. The increase in axial direction

tabulated in Table 4.4 is the increase in PEO/PUMVS layer thickness of hybrids 3-5 compared to hybrid 2. The increase is not compared to pure PI-*b*-PEO block copolymer or hybrid 1 as they exhibit a cylindrical and not a lamellar structure.

The TEM images and SAXS data analysis both show that with increasing PUMVS loading the PEO/ PUMVS layer thickness increases while the PI layer thickness decreases. The decrease in PI layer thickness can be related to the large degree of stretching induced in the PI block upon crystallization of the PEO block. Because the two blocks are covalently bound together and the constraint of constant density, if the PEO layer thickens upon crystallization, the amorphous PI chains must stretch to thicken the PI layer proportionally. The highly stretched conformation of the PI chains provides a driving force for the solubilization of PUMVS in the PEO block as the PI chains are allowed to relax to a more random coil conformation. The addition of PUMVS to the PEO block thus reduces the conformational free energy of the PI block and leads to a decrease in PI layer thickness.

The increase in PEO/PUMVS layer thickness with increasing PUMVS loading is due to the preferential swelling of the PEO chains with the PUMVS. The possibility of complete segregation of PUMVS in the middle of the PEO domain, and thereby simply increasing the volume, is excluded, because this kind of distribution does not lead to conformational changes in the block copolymer, i.e. no change in PI layer thickness would have been observed. However, the PUMVS does not necessarily swell the PEO chains throughout the PEO/PUMVS domain to the same extent, i.e. the PUMVS does not have to be uniformly distributed throughout the PEO/PUMVS layer.

To investigate the symmetry of the swelling, the average interfacial area per copolymer junction of the PI-*b*-PEO interface is calculated from SAXS data (assuming that the PUMVS does not penetrate the PI block and that the interface between the PI and PEO domains is narrow). The average area per chain junction for a lamellar

Table 4.4. Comparison of axial and lateral changes in the PEO/ PUMVS layer

Sample	PUMVS/ block copolymer weight ratio	PI layer thickness* (nm)	PEO/ PUMVS layer thickness* (nm)	Increase in axial direction (%)	Area per junction* (nm^2)	Increase in lateral direction (%)
2	0.55	15.7	10.5	-	5.14	-
3	1.05	12.7	14.6	38.5	6.36	11.2
4	1.96	9.2	18.7	77.5	8.72	30.3
5	2.50	8.4	21.3	102	9.59	36.6

* determined by SAXS

morphology is given by [23]:

$$\sigma_j = \frac{2M_{PI}}{N_{Av}\rho_{PI}(1-\Phi_{PEO/PUMVS})L} \tag{4.3}$$

where M_{PI} is the number average molecular weight of the PI block, N_{Av} is Avogadro's number and ρ_{PI} is the PI density. Whereas the individual layer thicknesses, calculated above, are a measure of the axial changes perpendicular to the PI-*b*-PEO interface, the area per junction is a measure of the lateral changes parallel to the PI-*b*-PEO interface. Figure 4.7a and 4.7b schematically illustrate lateral swelling versus axial swelling, respectively, in the PI-*b*-PEO/ PUMVS hybrids, and results of the calculations are summarized in Table 4.4.

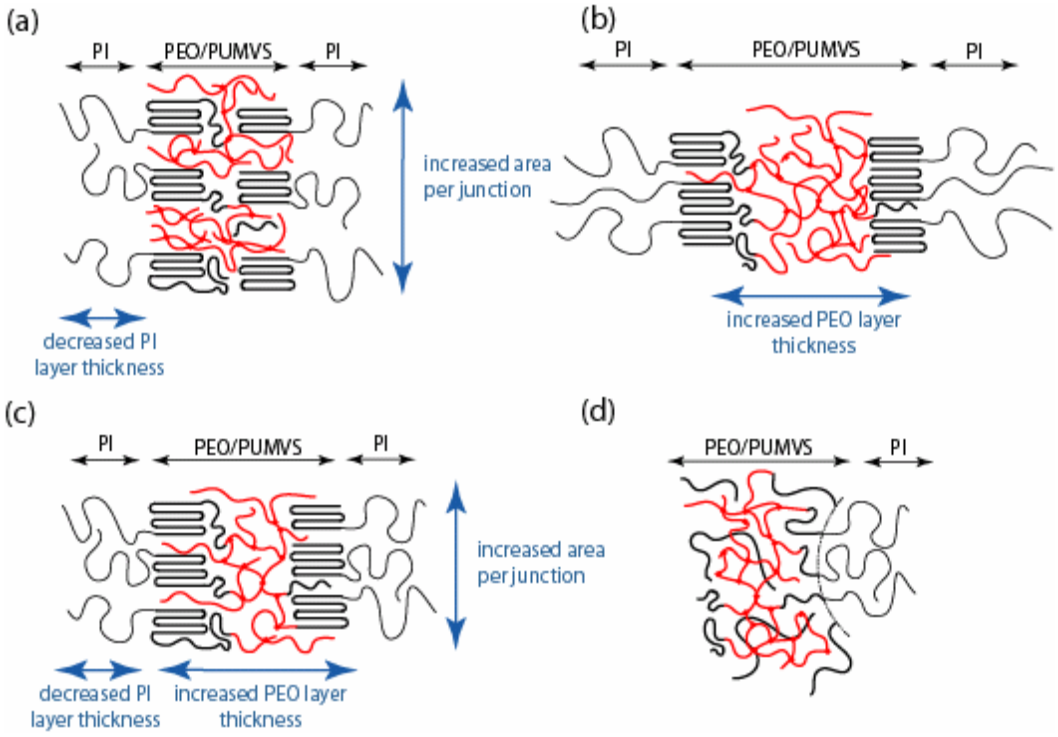

Figure 4.7. Schematic illustrating (a) lateral swelling, (b) axial swelling, (c) lamellar morphology in as-synthesized PI-*b*-PEO/PUMVS hybrid and (d) cylindrical morphology for annealed PI-*b*-PEO/PUMVS.

From Table 4.4, the area per junction increases upon increasing amount of PUMVS. Comparing the increase of the PEO/PUMVS layer thickness to the increase in area per junction of a hybrid gives an indication of the symmetry of the swelling. As was previously shown for blends of poly(isoprene–*block*–styrene) (PI–*b*–PS) diblock copolymers with polystyrene homopolymers [23-25], PS homopolymer (with molecular weights comparable to the PS block in the block copolymer) preferentially mixes with the PS block segments away from the PS-*b*-PI interface to prevent a loss in entropy for the homopolymer due to spatial constraints. In this PI-*b*-PS/PS system, upon increased loading of PS homopolymers, a lower bound plateau for the PI layer thickness and a limit for the lateral swelling were observed. In the present system the swelling of the lamellar PEO domains is also larger in the axial direction than in the lateral direction, indicating a non-uniform distribution of PUMVS within the lamellae, with the highest PUMVS segment density at the center of the lamellae. The changes in the present system are schematically represented in Figure 4.7c. However, no lower limit for the PI layer thickness or limit in lateral swelling is observed, even though both the molecular weight and the loading of the crosslinked PUMVS are much higher than that of the PS homopolymers in the earlier study.

The increased lateral swelling as compared to the PI-*b*-PS/PS system is caused by relaxation of the highly stretched PI chains, as described above. Therefore, the tendency for PUMVS localization at the domain centers is smaller for the present system compared to the PI-*b*-PS/PS system. The good structural regularity in the hybrids observed in TEM even upon high PUMVS loadings also indicates this. A high degree of lateral swelling was also found for blends of semicrystalline polyethylene-poly(ethylene-alt-propylene) diblock copolymers with semicrystalline polyethylene homopolymers [26]. This was explained by relief of chain stretching of the amorphous block as well. Thus, our data suggests that upon PUMVS loading the PI chain

stretching relaxes by swelling the PEO domains in the lateral direction, resulting in a smaller increase in the overall structural periodicity in the PI-*b*-PEO/PUMVS system relative to the amorphous PI-*b*-PDMAEMA/PUMVS system.

2.3. Order-order phase transitions

It was previously shown for a polybutadiene–*block*–poly(ethylene oxide) diblock copolymer/ PUMVS system [9, 10] that upon annealing at elevated temperatures the system could undergo order-order phase transitions leading to morphologies in the structural evolution beyond lamellar. As this system is very similar to the present system, annealing was explored in order to try out the same thing for the PI-*b*-PEO/ PUMVS system. To this end, a hybrid with a PUMVS/PI-*b*-PEO ratio of 2.3 (hybrid 11) was annealed at 300 °C for 5 hrs. The morphology of this annealed hybrid was investigated with SAXS and TEM and results compared to the as-synthesized material.

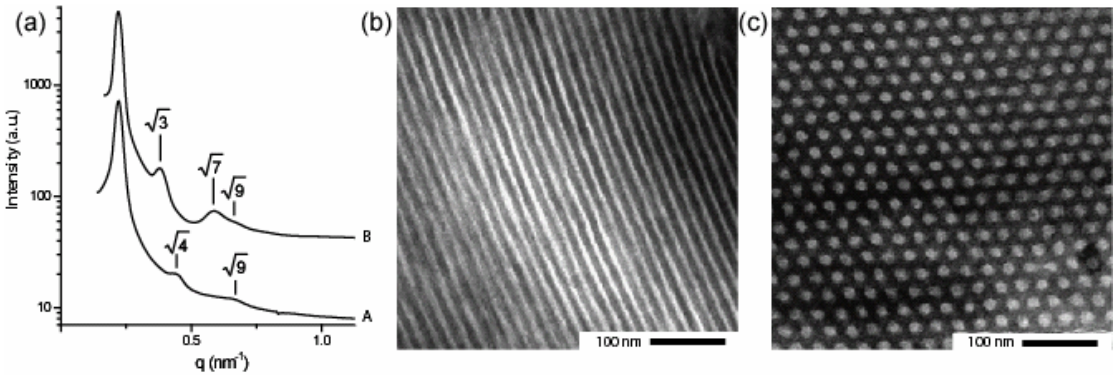

Figure 4.8. Morphology of PI-b-PEO/PUMVS hybrids subjected to different heat treatments. (a) SAXS traces for hybrid 11. A: as-synthesized; B: annealed at 300 °C. Bright-field TEM images of hybrid 11. (b): as-synthesized; (c): annealed at 300 °C.

Figure 4.8a shows the respective SAXS traces. As-synthesized hybrid 11 shows higher order reflections at angular positions of $\sqrt{4}$ and $\sqrt{9}$ of the first-order maximum, consistent with a lamellar morphology. This is corroborated by TEM

(figure 4.8b) and is consistent with the results discussed earlier, see Table 4.3 (compare samples 3, 4 and 11). The SAXS trace of the same sample after annealing at 300 °C shows higher order reflections at angular positions of $\sqrt{3}$, $\sqrt{7}$ and $\sqrt{9}$ of the first-order maximum, consistent with cylinders packed in a hexagonal lattice. The TEM image in figure 4.8c clearly shows the hexagonal packing of light (PI) cylinders in a dark (PDMAEMA/PUMVS) matrix. The TEM observations thus corroborate the interpretation of the SAXS data.

The effective PEO/PUMVS volume fraction of this hybrid is 0.70. Pure PI-*b*-PEO with a similar composition shows the same type of order-order phase transition upon heating [18]. But in case of the PI-*b*-PEO/PUMVS hybrid the system is prevented from going back to the crystalline lamellar morphology upon cooling to temperatures below the PEO crystallization temperature, see also schematic 4.7d. The DSC curve of hybrid 11 in Figure 4.5c does not show a melting peak, corroborating this hypothesis. This change in behavior is not due to polymer degradation. We cross-checked that pure PI-*b*-PEO after the same heat treatment still shows a strong melting peak in DSC. Rather, heating to higher temperatures first leads to PEO crystal melting and better mixing of PEO chains with the PUMVS. Upon further annealing at elevated temperatures the mobility of the PEO chains is expected to be diminished due to increased covalent coupling of the PEO chains to the PUMVS discussed earlier and to progressing crosslinking between the PUMVS molecules [27], adding barriers to crystallization.

Order-order phase transitions were also found in block copolymer epoxy-resin mixtures [5]. These transitions were caused by the local segregation of PEO out of the epoxy matrix. This results in a smaller effective PEO/epoxy volume fraction and therefore morphologies with flatter interfaces become more stable. The order-order phase transition observed in the present system is not a transition towards a flatter

interface and therefore cannot be explained by segregation of PEO out of the PUMVS matrix. The covalent bonding between the terminal hydroxy group of the PEO chain and the PUMVS is thought to prevent complete segregation between the PEO and the PUMVS.

Conclusions

The effect of using a semicrystalline diblock copolymer, PI-*b*-PEO, versus an amorphous block copolymer, PI-*b*-PDMAEMA, as structure directing agent for a polymer derived ceramic precursor, PUMVS, on hybrid morphology was investigated. The PUMVS preferentially swells the hydrophilic block of both block copolymers, and by systematically increasing the PUMVS/ block copolymer ratio a sequence of (up to four) morphologies were obtained from a single amorphous PI-*b*-PDMAEMA block copolymer, that is expected from typical block copolymer phase diagrams. However, in the case of PI-*b*-PEO a crystalline lamellar morphology is obtained for most PUMVS/ block copolymer ratios, upon crystallization of the PEO. The overall periodicity of the PI-*b*-PEO/ PUMVS hybrids increased only slightly upon PUMVS loading, because the strong chain stretching in the PI block is progressively relaxed as the PUMVS swells the PEO. Suppression of the crystallization through high temperature annealing results in morphological behavior similar to the amorphous PI-*b*-PDMAEMA/PUMVS system.

Acknowledgements

The authors thank Arthur Woll for help with the SAXS experiments and Lewis Fetters for discussions. The financial support of the National Science Foundation (award DMR-0605856) is gratefully acknowledged. The work was further supported by the Cornell Center for Materials Research (CCMR), a Materials Research Science

and Engineering Center of the National Science Foundation (DMR-0520404). CHESS is supported by the NSF & NIH/NIGMS via NSF award DMR-0225180.

REFERENCES

[1] M. Templin, A. Franck, A. DuChesne, H. Leist, Y. M. Zhang, R. Ulrich, V. Schadler, U. Wiesner, *Science* **1997**, *278*, 1795.

[2] P. Yang, D. Zhao, D. I. Margolese, B. F. Chmelka, G. D. Stucky, *Nature* **1998**, *396*, 152.

[3] Y. Wan, D. Y. Zhao, *Chemical Reviews* **2007**, *107*, 2821.

[4] M. A. Hillmyer, P. M. Lipic, D. A. Hajduk, K. Almdal, F. S. Bates, *Journal of the American Chemical Society* **1997**, *119*, 2749.

[5] P. M. Lipic, F. S. Bates, M. A. Hillmyer, *Journal of the American Chemical Society* **1998**, *120*, 8963.

[6] H. Kosonen, J. Ruokolainen, P. Nyholm, O. Ikkala, *Macromolecules* **2001**, *34*, 3046.

[7] C. B. W. Garcia, C. Lovell, C. Curry, M. Faught, Y. M. Zhang, U. Wiesner, *J. Polym. Sci. Pt. B-Polym. Phys.* **2003**, *41*, 3346.

[8] M. Kamperman, C. B. W. Garcia, P. Du, H. S. Ow, U. Wiesner, *Journal of the American Chemical Society* **2004**, *126*, 14708.

[9] J. L. Wan, A. Alizadeh, S. T. Taylor, P. R. L. Malenfant, M. Manoharan, S. M. Loureiro, *Chemistry of Materials* **2005**, *17*, 5613.

[10] J. Wan, P. R. L. Malenfant, S. T. Taylor, S. M. Loureiro, M. Manoharan, *Materials Science and Engineering A* **2007**, *463*, 78.

[11] E. M. Freer, L. E. Krupp, W. D. Hinsberg, P. M. Rice, J. L. Hedrick, J. N. Cha, R. D. Miller, H. C. Kim, *Nano Letters* **2005**, *5*, 2014.

[12] J. Allgaier, A. Poppe, L. Willner, D. Richter, *Macromolecules* **1997**, *30*, 1582.

[13] S. Renker, In *Doctoral dissertation*; Max Planck Institute for Polymer Research: Mainz, Germany, **2003**.

[14] S. Creutz, P. Teyssie, R. Jerome, *Macromolecules* **1997**, *30*, 6.

[15] M. Kamperman, P. Du, R. O. Scarlat, E. Herz, U. Werner-Zwanziger, R. Graf, J. W. Zwanziger, H. W. Spiess, U. Wiesner, *Macromolecular Chemistry and Physics* **2007**, *208*, 2096.

[16] M. W. Matsen, F. S. Bates, *Macromolecules* **1996**, *29*, 7641.

[17] A. K. Khandpur, S. Forster, F. S. Bates, I. W. Hamley, A. J. Ryan, W. Bras, K. Almdal, K. Mortensen, *Macromolecules* **1995**, *28*, 8796.

[18] G. Floudas, B. Vazaiou, F. Schipper, R. Ulrich, U. Wiesner, H. Iatrou, N. Hadjichristidis, *Macromolecules* **2001**, *34*, 2947.

[19] P. J. Holdsworth, A. Turner-Jones, *Polymer* **1971**, *12*, 195.

[20] P. J. Lemstra, G. Challa, T. Kooistra, *Journal of Polymer Science, Polymer Physics Edition* **1972**, *10*, 823.

[21] J. Brandrop, E. H. Immergut, *Polymer Handbook*; Wiley: New York, **1975**.

[22] CERASET SN Inorganic Polymer Technical Bulletin. Lanxide Company, **1997**.

[23] K. I. Winey, E. L. Thomas, L. J. Fetters, *Macromolecules* **1991**, *24*, 6182.

[24] T. Hashimoto, H. Tanaka, H. Hasegawa, *Macromolecules* **1990**, *23*, 4378.

[25] H. Tanaka, H. Hasegawa, T. Hashimoto, *Macromolecules* **1991**, *24*, 240.

[26] P. Rangarajan, C. F. Haisch, R. A. Register, D. H. Adamson, L. J. Fetters, *Macromolecules* **1997**, *30*, 494.

[27] Y. L. Li, E. Kroke, R. Riedel, C. Fasel, C. C. Gervais, C. F. Babonneau, *Applied Organometallic Chemistry* **2001**, *15*, 820.

CHAPTER 5

INTEGRATING STRUCTURE CONTROL ON EIGHT LENGTH SCALES IN POROUS HIGH TEMPERATURE CERAMICS WITH CATALYTIC FUNCTION[4]

Abstract

High temperature ceramics with porosity on multiple length scales offer great promise in high temperature catalytic applications, through their high surface area and low flow resistance in combination with thermal and chemical stability. We have developed a bottom-up approach to functional, porous high temperature ceramics structured on eight distinct length scales integrating catalytic activity from the near-atomic to the macroscopic level. Structuring is achieved through a combination of micromolding and multi-component colloidal self-assembly. The resulting template is filled with a solution containing a solvent, a block copolymer, a ceramic precursor and a nanoparticle catalyst precursor as well as a radical initiator. Heat treatment results in three-dimensionally interconnected, high temperature ceramic materials functionalized with well-dispersed 1-2 nm platinum catalyst nanoparticles and very high porosity.

[4] Kamperman, M.; Burns, A.; Weißgraeber, R.; van Vegten, C. H.; Warren, S. C., Gruner, S. M.; Baiker, A.; Wiesner, U.: to be submitted.

Nature exhibits phenomenal diversity and control in the structural design of materials, from cellulose aggregates in wood to silica nanostructures in diatom shells. These materials often integrate function through structural variations from the atomic scale all the way to the macroscale, tailored to create combinations of properties that are well-adapted to their purposes [1]. Structural control is commonly achieved starting from multi-component systems including macromolecules, such as proteins, peptides and polysaccharides that act as scaffolds or structure directing agents in assembly processes for inorganic materials [2]. A striking recently studied example is the marine glass sponge *Euplectella* sp., which produces integrated silica composite materials exhibiting at least seven hierarchical levels of structure to generate outstanding mechanical stability and toughness [3].

Fundamental understanding of a natural system challenges our ability to mimic Nature, with the guiding philosophy that the only way to understand how to build a house is to build one yourself. Despite considerable progress in the field of nanotechnology, integration of function from the atomic or near-atomic scale to the macroscopic scale remains a major challenge. To our knowledge no one had succeeded in bottom-up synthetic self-assembly of a material with seven or more hierarchical levels of structure in which a function is integrated, as observed in nature like for *Euplectella* sp.. Here we demonstrate a synthetic high temperature functional ceramic material prepared by soft matter assembly combining properties from eight components within a single highly porous material. We focus on catalytic functionality, since, it is widely recognized that hierarchically ordered pore structures in stable and robust catalyst supports are highly desirable. Macropores reduce flow resistance, allowing easy entry to the bulk of the material, where the large surface area of the mesopores can be effectively accessed.

A pioneering example, albeit without integrated function, of synthetically produced, porous oxide materials hierarchically ordered over three discrete length scales was an approach combining co-assembly of triblock copolymers and sol-gel species, with confined colloidal crystallization and micromolding [4, 5]. Subsequent approaches for production of hierarchically ordered materials included microporous zeolitic colloids used as building blocks within a macrotemplate [6, 7], combinations of polystyrene (PS) spheres, block copolymer and 'ionic liquid' templating [8], multi-component colloidal assembly [9, 10] and hierarchically ordered carbon [11, 12]. Unfortunately, the relatively low hydrothermal stability of mesoporous silica [13] and the combustibility of carbon in air at 500 °C [14] make these materials unsuitable for use in high temperature catalysis.

In contrast to oxide- and carbon-based porous materials structure directed by organic molecules, much less research has been conducted on porous non-oxide ceramics derived from self-assembled composites. As a result of their excellent thermal and chemical stability, non-oxide materials such as silicon carbonitride are promising candidates as supports for high temperature catalysts. To this end, ordered and non-ordered porous SiC and SiC_xN_y materials have been developed [15-17]. Impregnation of a macroporous SiC with a ruthenium salt resulted in a catalyst with high conversions for the decomposition of ammonia at temperatures above 700 °C, which make these structures interesting candidates for hydrogen production [18]. Functional integration in this case, however, was limited to two length scales and required multiple synthetic steps.

Here we present highly porous high temperature ceramic materials that are structured over eight discrete length scales and catalyze methane combustion. We combined micromolding and two-component colloidal self-assembly with cooperative assembly of a five component precursor system (solvent, amphiphilic block

copolymer, radical initiator, ceramic and platinum catalyst precursors) to obtain the desired materials. Heat treatment to 1000 °C led to three-dimensionally interconnected, hierarchically ordered, highly porous, high temperature ceramic materials functionalized with well-dispersed Pt nanoparticles. Experimental challenges that needed to be overcome included finding the right combination of colloidal particle sizes for the two-component colloidal crystal formation within the channels, selecting the right solvent providing high enough solubility for all solution components, but without dissolving the colloidal template, and optimizing the solution viscosity for the precursor infiltration process into the colloidal template.

Figure 5.1 shows a schematic illustrating the two-step process used to obtain the integrated materials. The first step involved the colloidal self-assembly of PS spheres of two sizes in microchannels defined by a poly(dimethylsiloxane) (PDMS) mold. The mold provided 500 μm wide channels open at both ends, with walls that integrated 60 μm wide channels. The mold was placed on a freshly cleaned Si wafer and a drop of PS sphere suspension in water was placed on one side of the mold. PS sphere sizes tested included combinations of 16.0, 3.0, 2.0 and 1.0 μm diameter spheres with 1.0 μm, 600, 350, 200 and 100 nm sized beads. The concentration ratios C_{small}/C_{large} were varied between 0.017 and 0.17. Best results were obtained with suspensions containing PS spheres with diameters of 3.0 μm and 350 nm in a concentration ratio of $C_{350nm}/C_{3\mu m} = 0.08$. Capillary action filled the channels with the colloidal suspension. Solvent evaporation from the open end of the channels acted as the driving force for sphere packing as the drying front progressed towards the reservoir side. The order and the type of binary lattice formed depended on the size, the size ratio and relative concentrations of the spheres and could be altered to control the density of the final materials [9, 19-22].

The second step in the process was the infiltration of the packed three component bed with the five component precursor solution, consisting of a solvent, an amphiphilic block copolymer, a ceramic precursor for SiCN type materials, a platinum nanoparticle precursor and a radical initiator. The challenge was to select the right solvent to ensure solubility of all components, even at high concentration (at the drying front), without dissolving the colloidal template. Initial experiments were pursued with tetrahydrofuran (THF) or toluene and crosslinked PS spheres. While

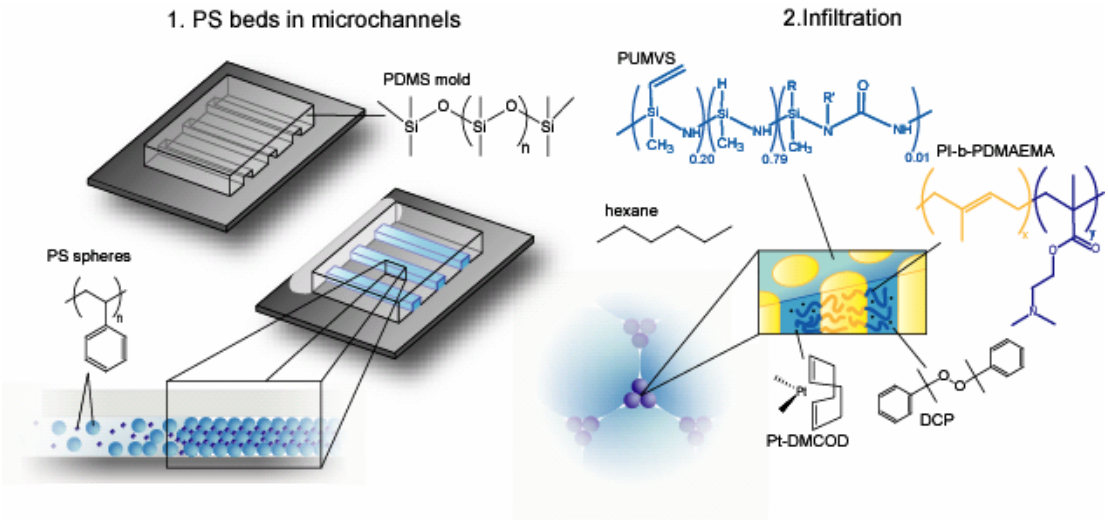

Figure 5.1. Schematic representation of the two step synthetic procedure. **(1)** Colloidal self-assembly of polystyrene spheres with two different diameters in the microchannels of a PDMS mold. **(2)** Infiltration of the packed three component bed with the five component precursor solution, consisting of amphiphilic block copolymer PI-*b*-PDMAEMA (PI is yellow and PDMAEMA is blue), ceramic precursor for SiCN type materials (PUMVS molecule has cyclic and linear features; R=H or vinyl, no information is available about the nature of R'), Pt nanoparticle precursor (Pt-DMCOD) and radical initiator all in hexane as solvent. Co-assembly leads to nanostructured morphologies that can be permanently set by crosslinking the PUMVS. Temperature treatment up to 1000°C results in a three-dimensionally interconnected, high temperature ceramic material structure directed on eight different length scales that is functionalized with well-dispersed platinum nanoparticles.

these are excellent solvents for many organic materials, they led to significant deformations of colloid shape. After trying many combinations of solvents and precursors we arrived at the following materials and solvent choices. The block copolymer poly(isoprene-*block*-dimethylaminoethyl methacrylate) (PI–*b*–PDMAEMA) was used as a structure directing agent for the polymeric ceramic precursor, poly(ureamethylvinyl)silazane (PUMVS) (see Figure 5.1 for molecular structures) [23]. PUMVS is a so-called polymer-derived ceramic (PDC), which starts out as a polymer that can be shaped into complex structures and solidified by cross-linking through polymerization with dicumyl peroxide as radical initiator. Heat treatment transforms the polymeric precursor into ceramic SiCN materials, while retaining the original (complex) shape [24-26]. Mixing PUMVS with this block copolymer was expected to lead to preferential swelling of the hydrophilic PDMAEMA domains with PUMVS due to its polar nature [15]. To generate an inverse hexagonal morphology, with PI cylinders in a PUMVS/PDMAEMA matrix, a PI-*b*-PDMAEMA block copolymer with a total molecular weight of 31 kg/mol and 33 wt% PDMAEMA was mixed with PUMVS in a 1:2 ratio in hexane [27]. Dicumyl peroxide and (1,5-cyclooctadiene) dimethylplatinum (Pt-DMCOD) were added to the solution as radical initiator (to crosslink the PUMVS) and Pt nanoparticle precursor, respectively. Platinum was expected to preferentially segregate in the PDMAEMA domains, as the allyl groups of the PUMVS can efficiently add to Pt [28], in a similar fashion to the double bond coordination of Pt with cyclooctadiene in the precursor molecule (see Figure 5.1 for the molecular structures of the ceramic and catalyst precursors) [29]. A drop of this solution was placed on one side of the mold leading to interstitial space filling between the PS spheres by capillary action.

Another experimental challenge was optimizing the precursor solution viscosity. The viscosity had to be low enough to maintain porosity on all levels at the

interface between the PDMS mold and the colloidal crystal, preventing a 'closed' interface limiting the accessibility of the inner pores inside the channels in the final material. On the other hand, the viscosity had to be high enough to prevent lifting off of the mold from the Si substrate, in which case the integrity of the channel structure would have been lost. The largest contribution to solution viscosity arises from the polymers. Fixing the block copolymer: PUMVS ratio at 1:2, we varied the polymer (PI-*b*-PDMAEMA + PUMVS): hexane weight ratio between 0.15:1 and 0.60:1. Best results were obtained for a weight ratio of 0.5:1. The structure was permanently set by PUMVS crosslinking by the radical initiator at 130 °C. Careful removal of the mold and subsequent heat treatment under reducing atmosphere to 1000 °C simultaneously removed organic volatiles, converted the PUMVS into a ceramic, and reduced the Pt-precursor to its metallic form.

The final material shows ordering on eight distinct length scales as summarized in Figure 5.2. The upper part of Figure 5.2 (A-I) shows experimental imaging results while the lower part (J-Q) depicts the eight structural levels in an illustration. On the macroscopic scale (5 mm) the shape of the sample is governed by the shape and size of the mold (Figure 5.2A, J). The ability to mold porous materials into any desired shape and size increases the range of applications significantly compared to a powder. The second and third levels of ordering (500 and 60 μm) are the microchannel patterns created by the micromold (Figure 5.2K, L). Figure 5.2B shows a light microscope image and Figures 5.2C and 2D show scanning electron microscopy (SEM) images of the heat treated material, demonstrating the quality of the channel reproduction. The fourth and fifth structural levels of ordering are controlled through colloidal crystal templating through two sizes of polystyrene particles (Figure 5.2E, F, M and N). The 3.0 μm latex spheres self-assembled into a close-packed lattice and the smaller 350 nm latex spheres were forced to pack into the

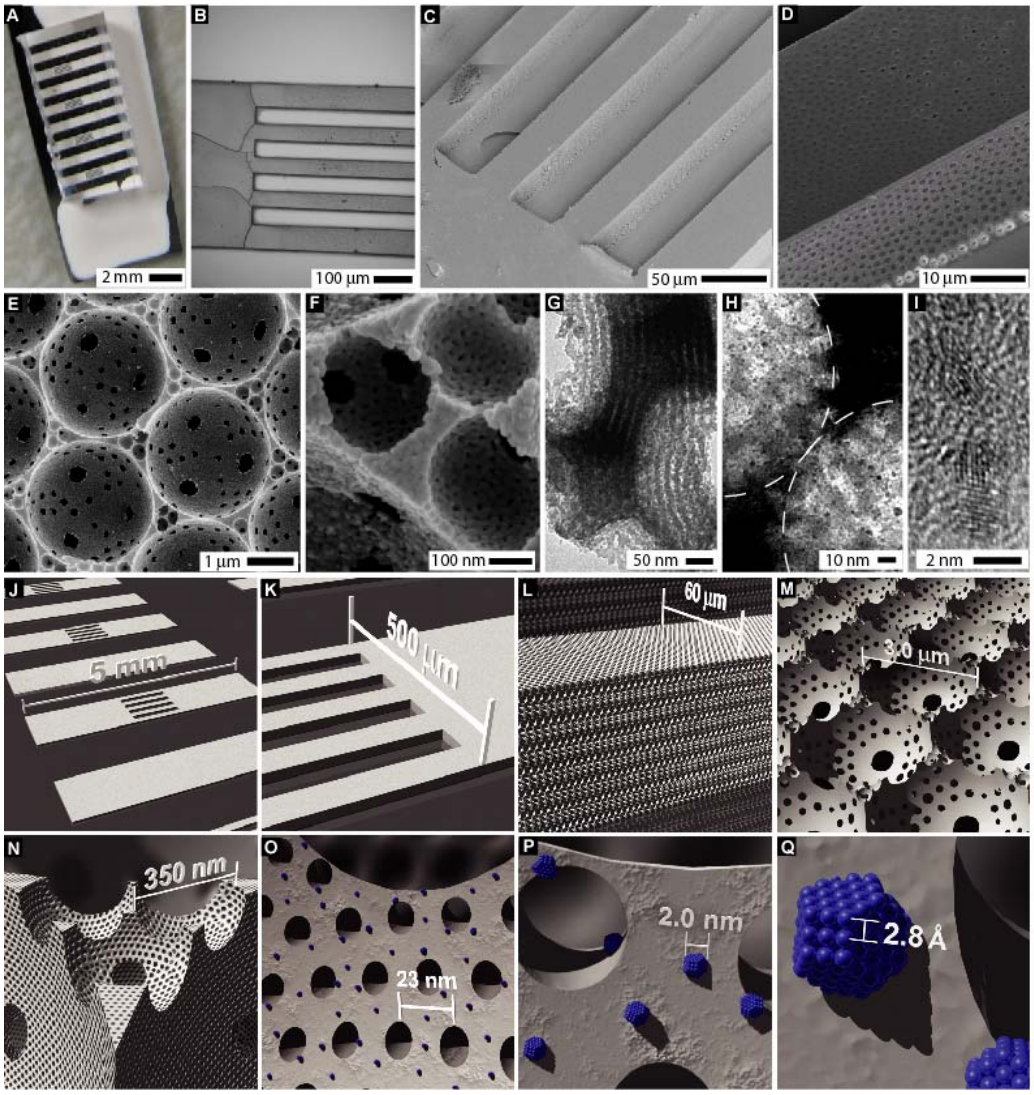

Figure 5.2. Analysis of material structured on eight discrete length scales. **(A)** Photograph showing the shape and size of the mold. **(B)** Light microscope image and **(C,D)** scanning electron microscopy (SEM) images of the channel structures. **(E)** SEM showing channels with a binary colloid-templated structure, consisting of 2.7 µm and 0.29 µm sized holes. **(F)** SEM zooming in on the interstitial space of the large colloids revealing that the framework of the porous structure is itself an ordered mesoporous material due to the co-assembly of the block copolymer and the PUMVS. **(G)** Transmission electron microscopy (TEM) images of a crushed sample showing the average distance between mesopores of 25 nm. **(H)** TEM image showing 1-2 nm diameter Pt nanoparticles distributed throughout the material. Dotted lines indicate the colloidal crystal templated structure as a guide. **(I)** High resolution TEM resolving Pt lattice fringes. Schematic representation of the eight structural levels in the final material. **(J)** Level 1: Macroscopic sample dimension; **(K, L)** Levels 2 and 3: Two different microchannel sizes; **(M, N)** Levels 4 and 5: Two-component colloidal self-assembly; **(O)** Level 6: Micro-phase separation of the co-assembled block copolymer and PUMVS; **(P)** Level 7: Pt nanoparticle size; **(Q)** Level 8: Pt crystal lattice spacing.

interstices between the large micron-spheres. The close-packed arrangement of the PS spheres (touching spheres) resulted in interconnecting, uniform-sized windows, giving rise to additional pore sizes, as can be clearly seen in Figures 5.2E and F.

The sixth structure level is determined by the mesopores of the framework itself, due to the microphase separation of the co-assembled block copolymer and PUMVS into an inverse hexagonal pore structure (see SEM image in Figure 5.2F and TEM image in Figure 5.2G as well as illustration 5.2O). The characteristic pore-to-pore distance was approximately 25 nm as estimated from TEM and SEM. The mesoporous nature of the pyrolyzed materials was confirmed by nitrogen physisorption (see Figure 5.3A). The material exhibits a type IV nitrogen sorption isotherm with specific surface area of 44 m^2/g. Barrett-Joyner-Halenda (BJH) pore size distribution, as derived from the nitrogen adsorption isotherm, reveals a uniform peak mesopore diameter of 11.0 nm [30], in agreement with pore size estimates from SEM and TEM images (see Figure 5.2F, 5.2G and 5.2H, respectively). Small angle X-ray scattering (SAXS) confirms mesoporous ordering (see Figure 5.3B,a). The first order peak ($q^* = 3.15 \times 10^{-2}$ $Å^{-1}$) corresponds to a repeat spacing of 19.9 nm while the second and third order peaks at $3^{½}$ and $7^{½}$ times q* are consistent with a hexagonal lattice. The lattice parameter results in a pore-to-pore distance of 23.0 nm in good agreement with both SEM and TEM data.

The material shrank during heat treatment, resulting in a decrease in channel width (measured at the top surface) of 7-11% and a decrease in pore size from the colloidal crystal templating of 10-17% compared to the original PS sphere sizes, as determined from SEM images. The hexagonal lattice spacing decreased by 30% compared to as-synthesized bulk PI-*b*-PDMAEMA/PUMVS hybrid materials. The lattice spacings were not directly compared to infiltrated packed bed samples as the diffuse scattering of the PS spheres made quantitative spectral analysis difficult. The

difference in shrinkage on the different length scales may in part be due to anisotropic behavior induced by the strong anchoring of the structure onto the Si substrate. This is suggested by earlier analysis of block copolymer-inorganic hybrid films subjected to heat treatments, showing uniaxial shrinkage as high as 30% along an axis perpendicular to the substrate surface [31].

After heat treatment under a reducing atmosphere to 1000 °C higher resolution TEM images reveal Pt nanoparticles homogeneously distributed throughout the walls of the material giving rise to the seventh structural level (Figure 5.2H, illustration 2P and Figure 5.4A and B). While metal compound loading is usually kept low to avoid negative influence of additives on the structure formation [32], in the present system Pt loadings of 5 wt% in the final material did not disrupt the order (see Figure 5.3B and Figure 5.4). Surprisingly, the particle size was found narrowly distributed around 1-2 nm in diameter. This is quite remarkable considering the high temperature treatment. Impregnated systems, even Pt-alumina catalysts that are commonly used, show much larger particle sizes (> 50 nm) after heat treatment to only 800 °C [33]. We further examined the material with powder X-ray diffraction (XRD) to determine the crystallinity of the Pt (see Figure 5.3C, a). The crystallite size as calculated from the Scherrer equation was 1.1 nm. The crystallinity of the particles was confirmed by high resolution transmission electron microscopy (HRTEM). The typical lattice spacing, measured from images like Figure 5.2i, was 2.2 Å, which is close to the lattice spacing of 2.26 Å expected for face-centered-cubic (f.c.c.) {111} lattice fringes in platinum. The lattice spacings of the Pt crystals (Figure 5.2Q) constitute the eighth and smallest structural level of our materials.

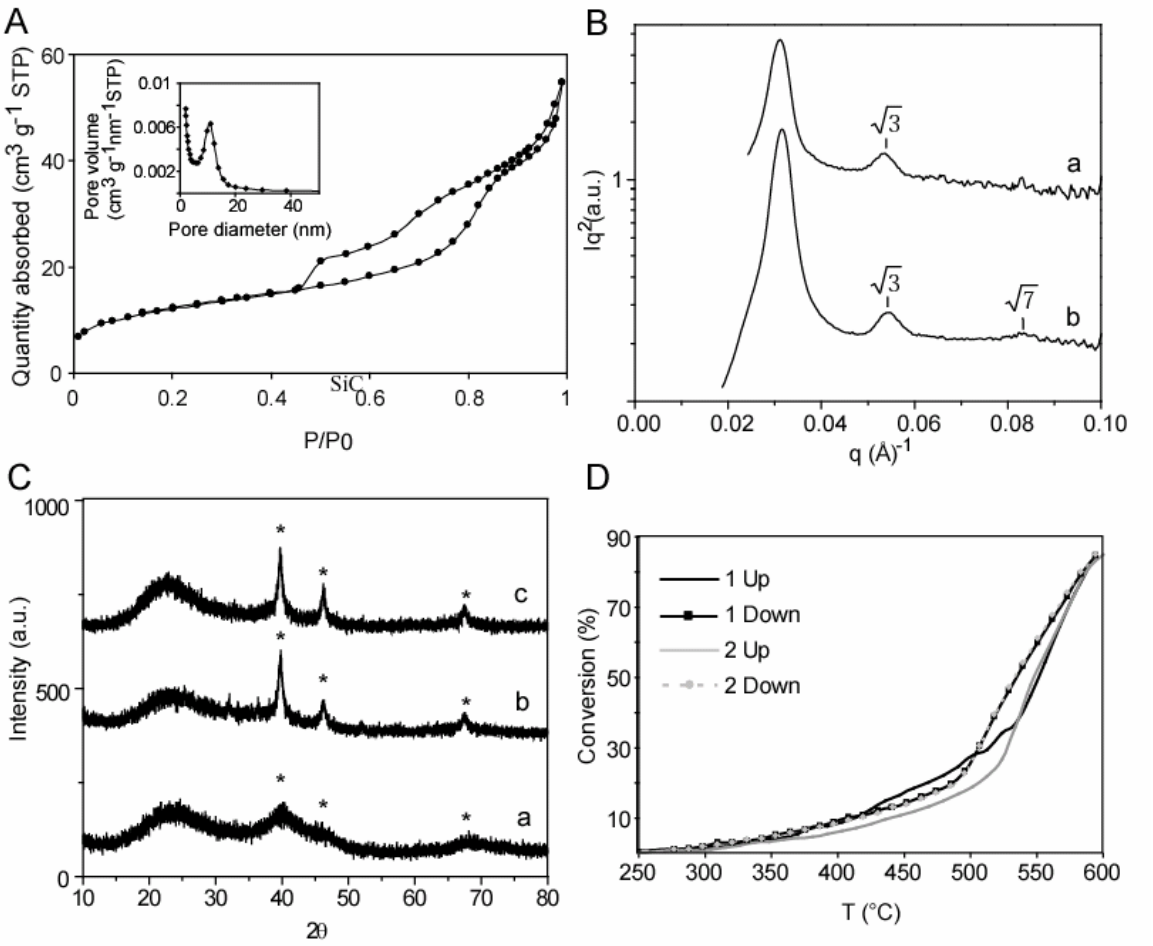

Figure 5.3. (A) Nitrogen adsorption–desorption isotherm with inset showing corresponding BJH pore size distribution calculated using the adsorption isotherm. **(B)** SAXS profiles of material heat treated to 1000 °C under an inert atmosphere (a) and after post heat treatment to 600 °C in air (b). Tic marks indicate positions of expected reflections for a hexagonal lattice. **(C)** Powder XRD patterns of (a) material heat treated to 1000 °C showing Pt nanoparticles with domain sizes of 1.1 nm, (b) material post heat treated to 600 °C in air for one minute showing Pt nanoparticles with domain sizes of 10.2 nm and (c) material post heat treated to 600 °C in air for an additional 10 hrs showing Pt nanoparticles with domain sizes of 11.0 nm. Expected Pt peaks are labeled with asterisks. **(D)** Methane conversion (activity) as a function of the reaction temperature during two heating/cooling cycles . Conditions: 15 mg of ceramic material, feed gas composition: 1 vol% CH_4, 4 vol% O_2 in balance He, total flow rate 130 mL/min, heating and cooling rate 2.5^{o}C/min. Other conditions and the experimental procedure are specified in Supporting Material.

The stability of the framework, sintering of the catalyst and catalytic activity of these materials were tested up to 600 °C in an oxidizing environment.

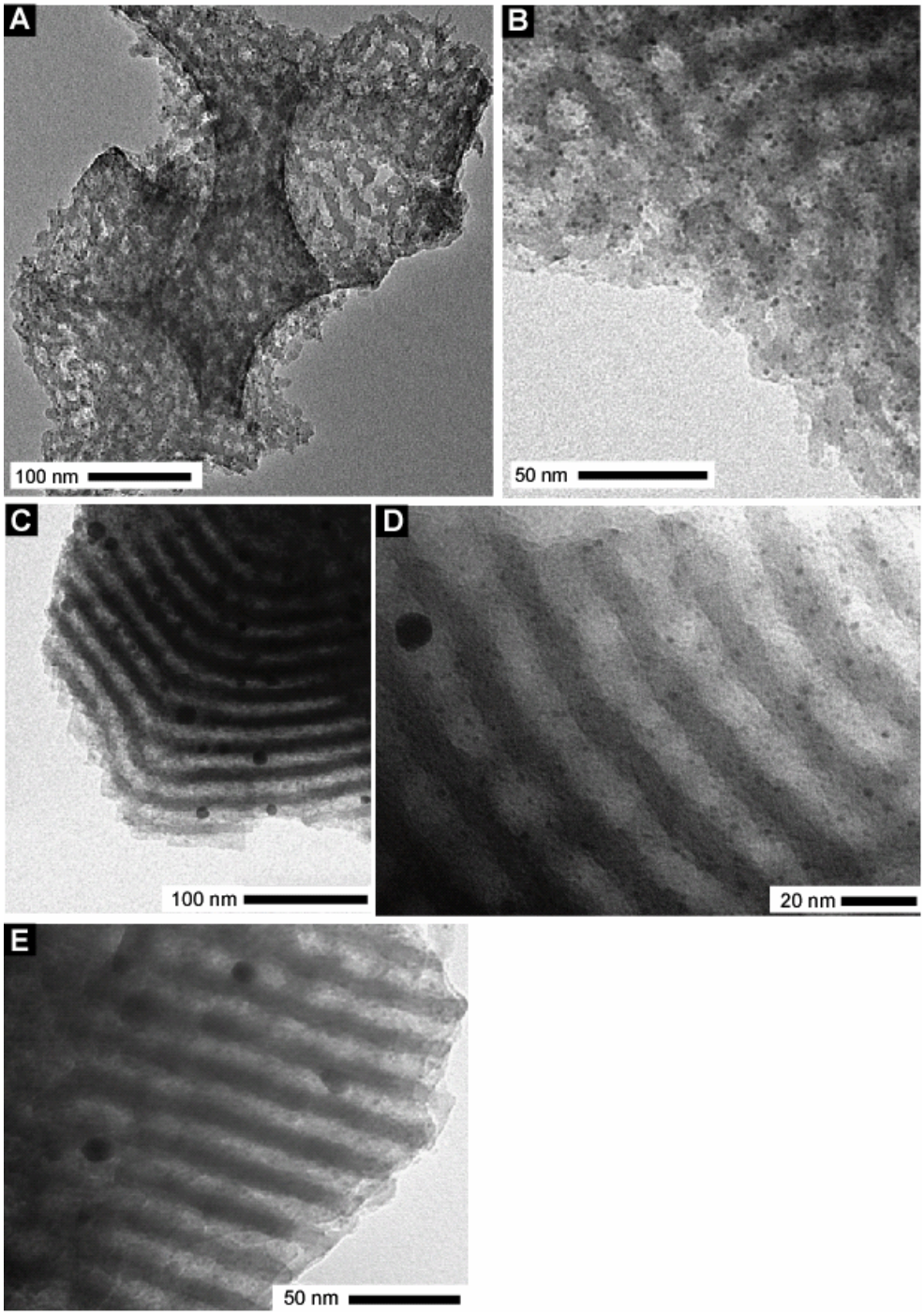

Figure 5.4. (A,B) TEM images showing the Pt nanoparticles homogeneously distributed throughout the material. **(**C,D) TEM images of material post heat treated to 600 °C in air for 1 minute and (E) for an additional 10 hrs.

Thermogravimetric analysis (TGA) under these conditions revealed that the weight of the pyrolyzed structure did not change substantially (see Figure 5.5) exhibiting a loss

of less than 5%, which was most likely due to gradual desorption of water below 350 °C, combustion of residual carbon in the material between 350 – 550 °C and the formation of a passivating oxide layer at the surface at around 575 °C. That the order was retained was verified by SAXS. The repeat spacing slightly increased by 0.3 nm to 20.2 nm, which is within the range of variation between samples (see Figure 5.3B,b). TGA and SAXS data thus confirm that the material is physically stable under oxidizing conditions up to temperatures at least as high as 600 °C in air. Catalyst sintering was investigated with a combination of TEM and XRD, comparing materials kept at 600 °C in air for 1 minute with materials reheated and maintained at 600 °C in air for an additional 10 hours. After only 1 minute at 600 °C a few larger particles of around 10 nm were observed next to the 1-2 nm ones in TEM (see Figure 5.4C and D) with a crystallite size of 10.2 nm as calculated from the XRD data using the Scherrer equation (see Figure 5.3C,b). After an additional 10 hrs at 600 °C only a slight further increase in the crystallite size to 11.0 nm was calculated from the XRD profile and corroborated with TEM (see Figures 5.3C,c and 5.4E). Interestingly, 11 nm is also the size of the mesopores, suggesting that the framework may prevent further particle growth beyond the confines of the mesopores. For the particular case where the Pt particles block the mesopores, a hierarchical pore structure is ideal for its ability to prevent loss of activity by providing multiple access routes to the catalyst.

The catalytic activity and thermal stability of the mesoporous ceramics was tested in the total oxidation of methane (combustion) [34], a reaction relevant to energy technology and environmental catalysis. Figure 5.3D presents the catalytic activity (conversion) as a function of the reaction temperature for two heating-cooling cycles. The methane conversion vs. temperature plots show the typical hysteresis behavior observed for the platinum-catalyzed methane oxidation during heating and subsequent cooling cycles. The almost identical curves for the cooling cycles suggest

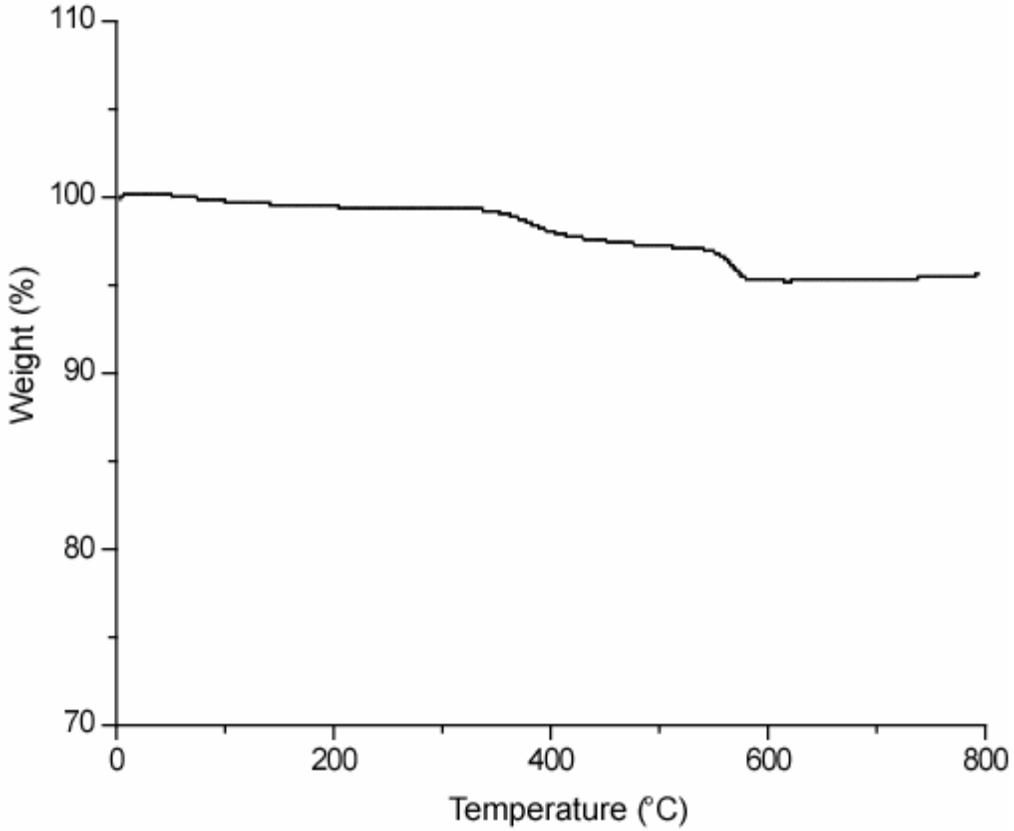

Figure 5.5. TGA analysis of ceramic material, heated at 5 °C/min to 850 °C under flowing air.

that the catalytic activity of the material became stable after the first heating cycle. The strong change of the slope of the conversion vs. time curve around 540 °C, is probably due to a change of the reaction mechanism induced by the transition from PtOx surface species to metallic Pt upon heating to higher temperatures. The catalytic tests clearly showed the potential of the developed ceramics for catalytic applications at high temperature such as methane oxidation. The system combines excellent size control and high thermal stability of the catalytically active platinum with high structural flexibility rendering this system especially interesting for size-selective catalysis, monolith- and microreactor applications.

The final materials exhibited very high porosities. For example, values of 87% and 94% void space were obtained for the system described in Figure 2, excluding or including the micromold channels, respectively (see calculation in the supporting online material). To the best of our knowledge these values represent the highest porosities yet obtained for materials with ordered pores. Such high porosities are typically only obtained in foams and aerogels [35]. However, the use of monolithic aerogels and foams is limited to static environments by their low tensile strength, resulting from significant variations in the ratio of wall thickness to pore size and stress concentrations at interparticle necks [36]. In contrast, the walls of the present materials are much more uniform, which may result in superior strength.

Experimental Section

Materials and Methods

Block copolymer synthesis. The poly(isoprene-block-dimethylaminoethylmethacrylate) (PI-*b*-PDMAEMA) was polymerized by anionic polymerization as previously reported [37, 38]. Gel permeation chromatography (GPC) was used to determine the molecular weight of the first block (polyisoprene, PI) and the polydispersity of the block copolymer. ^{1}H NMR was used to determine the overall molecular weight of the block copolymer. The resulting polymer had a molecular weight of 31 kg/mol comprised of 33 wt.-% PDMAEMA with a net polydispersity of 1.04.

Packed beds of PS spheres in PDMS microchannels. To make the PDMS molds a silicon master was photolithographically replicated as described elsewhere [39]. Polystyrene (PS) spheres were purchased from Polysciences and used as received. A 2.7 wt % suspension of the 3 μm PS spheres was concentrated to a 15 wt

% solution. 350 nm PS spheres (2.7 wt% in water) were added to the 3 μm PS spheres, resulting in a relative concentration ratio of $C_{350nm}/C_{3\mu m}$ of 0.08. The suspension was sonicated for 1 min to ensure complete dispersion of the particles. Silicon substrates were soaked in freshly prepared piranha solution (Concentrated H_2SO_4 and 30 wt % H_2O_2, in a 2:1 v/v mixture) for 30 min, rinsed several times with water, and dried under flowing nitrogen. The PDMS mold was mounted on the freshly cleaned substrate and placed on a hotplate at 30 °C. A drop of PS sphere suspension (20 μl) was placed at one end of the channels and left for several hours to complete the packing process [40].

Larger colloidal crystals for physisorption, powder X-ray diffraction (XRD), stability and activity measurements were made by convective assembly. A 1.2 wt% suspension of 3 μm and 350 nm PS spheres with a relative concentration ratio of $C_{350nm}/C_{3\mu m}$ of 0.08 was placed in a vial and sonicated for 1 min to ensure complete dispersion of the particles. The solution was transferred to a glass Petri dish and freshly cleaned substrates were dipped diagonally into the particle solution. The setup was placed in an oven at 60 °C. Samples were left overnight until the liquid evaporated.

Infiltration. The five component infiltration solution consisted of hexane as a solvent, the block copolymer (PI-*b*-PDMAEMA), the ceramic precursor, a radical initiator and the catalyst nanoparticle precursor. The (1,5-cyclooctadiene) dimethylplatinum (Pt-DMCOD) was synthesized as described previously [41]. The anhydrous hexane (Aldrich), the ceramic precursor, Ceraset (KiON Corp.) and the radical initiator, dicumyl peroxide (Aldrich) were used as received.

In a typical synthesis, 0.10 g of block copolymer was dissolved in 0.6 g anhydrous hexane in a 20 mL vial. 0.20 g of the ceramic precursor was added and the solution was stirred for 1h. Next, 0.0141 g Pt-DMCOD and 0.009 g radical initiator (1

wt.-% with respect to the mass of PUMVS added) were added and the vial was stirred for another 15 min. A drop of the block copolymer/ precursor solution was subsequently placed at one side of the PDMS mold. Samples were left for several hours until the liquid evaporated followed by crosslinking of the PUMVS at 130 ºC for 3 h. All steps (preparation of the solution, infiltration and crosslinking of the ceramic precursor) were carried out in a glove box under a nitrogen atmosphere owing to the sensitivity of the PUMVS to moisture [27]. The composite was finally heat treated using 1 ºC/min ramps under argon 95%/hydrogen 5% up to 1000 ºC for conversion into the high-temperature ceramic material and reduction of the catalyst.

Stability tests. Materials were reheated using 5 ºC/min ramps in air up to 600 ºC.

Structure Characterization

Electron Microscopy (SEM, TEM and HRTEM). The films were sputtered with gold before being characterized with SEM. SEM images were obtained on a LEO 1550 field-emission scanning electron microscope. For TEM, samples were crushed and then dispersed in ethanol. Bright field TEM micrographs were taken on a Tecnai T12 Spirit Twin TEM/STEM operating at 120 kV and high resolution energy filtered (zero loss) TEM was performed on a Tecnai F20 with a Gatan Tridium Spectrometer at 200 kV.

Small Angle X-Ray Scattering (SAXS) data were collected on a Rigaku RU300 copper rotating anode X-ray spectrometer ($\lambda = 1.54$ Å) operated at 40 kV and 50 mA. X-rays were monochromated with a Ni filter and focused using orthogonal Franks mirrors. SAXS patterns were collected with a homebuilt 1 K × 1 K pixel CCD detector similar to that described in [42].

PXRD was performed on a Scintag XDS 2000, with a scan rate of 0.1°/minute.

Thermogravimetric Analysis (TGA) was performed using a Netzsch Jupiter 449 C instrument with a gas flow of 50 mln/min of 20%O_2 in He.

Physisorption was performed on a Micromeritics ASAP 2020 using nitrogen as the adsorption gas.

Catalytic Tests were carried out by mixing 15 mg of the 100 – 200 μm fraction of the catalyst with 70 mg α-Al_2O_3 of 100-200 μm. This mixture was shaken until a homogeneous mixture was obtained, which was subsequently loaded into a quartz U-tube with an inner diameter of 5 mm. The catalyst bed was fixed by quartz wool plugs. The quartz U-tube was placed in a tubular oven (Carbolite Furnaces) and connected to a mass flow controller (Brooks, 5895E) and gas chromatograph (Hewlett Packard 6890N, equipped with GS GasPro column and capable of automatic gas sampling) by Swagelok couplings with Teflon O-rings. A manometer was used to monitor the pressure before the catalyst bed, which was constant at 0 barg during all experimental conditions.

Each catalytic experiment consisted of two cycles from 200 to 600°C and back with a heating and cooling ramp of 2.5 °C/min. Prior to each run, the catalyst was pre-treated at 200 °C in the reaction mixture of 1 vol% CH_4, 4 vol% O_2 in balance He. The total flow during each run was 130 mL/min. The experimental conditions were set so that the conversion never reached 100%. Carbon dioxide was the only reaction product detected. Blanc experiments demonstrated that the diluent, α-Al_2O_3 was not active under the chosen conditions.

Porosity. The porosity was calculated assuming the housing around the monolith would fit just around the sample. The 12 small and 6 large air-channels in this volume give rise to a porosity of:

$$\phi_{ch} = \frac{V_{sc} + V_{lc}}{V_{sample}} = \frac{12 \cdot 60 \cdot 950 + 6 \cdot 500 \cdot 5000}{12 \cdot 500 \cdot 5000} = 0.52 \qquad (5.1)$$

where ϕ_{ch} is the porosity from the channels, V_{sc} is the volume of the small channels, V_{lc} is the volume of the large channels and V_{sample} is the volume of the entire sample. The porosity due to the colloidal crystal templating was calculated assuming the large spheres pack in a fcc lattice. Calculations and experimental SEM data showed that for a sphere size ratio of 350 nm/3.0 μm = 0.117 one tetrahedral site can hold 20 small spheres and an octahedral site 69. There are two tetrahedral sites and one octahedral site for each large sphere. Therefore:

$$\phi_{cc} = \frac{4\left(\frac{4}{3}\pi r_{large}^{\ 3} + (2 \cdot 20 + 69)\frac{4}{3}\pi r_{small}^{\ 3}\right)}{V_{fcc}} = 0.84 \qquad (5.2)$$

where ϕ_{cc} is the porosity from the colloidal crystal, V_{fcc} is the volume of one cubic fcc unit cell and r_{large} (1350 nm) and r_{small} (145 nm) the radius of the large and small spheres, respectively. The mesopores in the wall gave rise to porosity of the framework. From the lattice parameter determined by SAXS (19.9 nm) together with the BJH average pore size (11 nm) an additional porosity of:

$$\phi_m = 0.21 \qquad (5.3)$$

arose, where ϕ_m is the porosity from the mesoporous framework.

The overall porosity of the material including the micromold channels is therefore:

$$\phi_{total} = \phi_{ch} + (1-\phi_{ch})\phi_{cc} + (1-((1-\phi_{ch})\phi_{cc} + \phi_{ch}))\phi_m = 0.94 \qquad (5.4)$$

and the overall porosity of the material excluding the micromold channels is:

$$\phi_{total} = \phi_{cc} + (1-\phi_{cc})\phi_m = 0.87 \qquad (5.5)$$

Acknowledgements

The authors thank Shahyaan Desai for help with the PDMS mold synthesis, Judy Cha for help with the HRTEM experiments and Chris Orilall for help with the XRD experiments. Poorna Rajendran and Ian Hosein are acknowledged for

discussions on colloidal assembly. The financial support of the National Science Foundation (award DMR-0605856) is gratefully acknowledged. This work made use of the Soft Matter Cluster and the Integrated Advanced Microscopy facilities of the Cornell Center for Materials Research (CCMR) with support from the National Science Foundation Materials Research Science and Engineering Centers (MRSEC) program (DMR 0520404).

REFERENCES

[1] E. Baer, A. Hiltner, R.J. Morgan*, Physics Today* **1992**, 45, 60.

[2] S. Mann, *Biomineralization: Principles and Concepts in Bioinorganic Materials*, Oxford University Press, Oxford, **2001**.

[3] J. Aizenberg *et al.*, *Science* **2005,** *309*, 275.

[4] P. D. Yang *et al.*, *Science* **1998,** *282*, 2244.

[5] Z. Y. Yuan, B. L. Su, *Journal of Materials Chemistry* **2006,** *16*, 663.

[6] B. T. Holland, L. Abrams, A. Stein, *Journal of the American Chemical Society* **1999,** *121*, 4308 .

[7] L. M. Huang *et al.*, *Journal of the American Chemical Society* **2000,** *122*, 3530.

[8] D. B. Kuang, T. Brezesinski, B. Smarsly, *Journal of the American Chemical Society* **2004,** *126*, 10534.

[9] J. J. Wang, Q. Li, W. Knoll, U. Jonas, *Journal of the American Chemical Society* **2006,** *128*, 15606.

[10] Z. Zheng *et al.*, *Journal of the American Chemical Society* **2008,** *130*, 9785.

[11] A. Taguchi, J. H. Smatt, M. Linden, *Advanced Materials* **2003,** *15*, 1209.

[12] G. S. Chai, I. S. Shin, J. S. Yu, *Advanced Materials* **2004,** *16*, 2057.

[13] F. Q. Zhang *et al.*, *Journal of Physical Chemistry B* **2005,** *109*, 8723.

[14] R. Ryoo, S. H. Joo, S. Jun, *Journal of Physical Chemistry B* **1999,** *103*, 7743.

[15] M. Kamperman, C. B. W. Garcia, P. Du, H. S. Ow, U. Wiesner, *Journal of the American Chemical Society* **2004,** *126*, 14708.

[16] I. K. Sung, Christian, M. Mitchell, D. P. Kim, P. J. A. Kenis, *Advanced Functional Materials* **2005,** *15*, 1336.

[17] K. Sonnenburg *et al.*, *Physical Chemistry Chemical Physics* **2006,** *8*, 3561.

[18] Christian, M. Mitchell, D. P. Kim, P. J. A. Kenis, *Journal of Catalysis* **2006,** *241*, 235.

[19] P. Bartlett, R. H. Ottewill, P. N. Pusey, *Physical Review Letters* **1992,** *68*, 3801.

[20] K. P. Velikov, C. G. Christova, R. P. A. Dullens, A. van Blaaderen, *Science* **2002,** *296*, 106.

[21] V. Kitaev, G. A. Ozin, *Advanced Materials* **2003,** *15*, 75.

[22] M. E. Leunissen *et al.*, *Nature* **2005,** *437*, 235.

[23] M. Templin *et al.*, *Science* **1997**, *278*, 1795.

[24] S. Yajima, J. Hayashi, M. Omori, *Chemistry Letters* **1975**, 931.

[25] Y. L. Li *et al.*, *Applied Organometallic Chemistry* **2001,** *15*, 820.

[26] S. R. Shah, R. Raj, *Acta Materialia* **2002,** *50*, 4093.

[27] M. Kamperman *et al.*, *Macromolecular Chemistry and Physics* **2007,** *208*, 2096.

[28] F. R. Hartley, *Chemical Reviews* **1969,** *69*, 799.

[29] Pt can also act as a catalyst for hydrosilation reactions coupling Si-H to C=C in PUMVS [28].

[30] E. P. Barrett, L. G. Joyner, P. P. Halenda, *Journal Of The American Chemical Society* **1951,** *73*, 373.

[31] A. C. Finnefrock, R. Ulrich, G. E. S. Toombes, S. M. Gruner, U. Wiesner, *Journal Of The American Chemical Society* **2003**, *125*, 13084.

[32] L. M. Bronstein, *Colloid Chemistry 1* **2003,** *226*, 55.

[33] T. Osaki, K. Nagashima, K. Watari, K. Tajiri, *Catalysis Letters* **2007,** *119*, 134.

[34] P. Gelin, M. Primet, *Applied Catalysis B-Environmental* **2002**, *39*, 1.

[35] CRC Press., *Handbook of Chemistry and Physics,* [HTML and PDF Electronic annual] **1999.**

[36] Woignier, T., et al., *Journal of Non-Crystalline Solids*, **1992**, *147*, 672.

[37] S. Renker, Max Planck Institute for Polymer Research, **2003**.

[38] S. Creutz, P. Teyssie, R. Jerome, *Macromolecules* **1997,** *30*, 6.

[39] D. C. Duffy, J. C. McDonald, O. J. A. Schueller, G. M. Whitesides, *Analytical Chemistry* **1998,** *70*, 4974.

[40] E. Kim, Y. N. Xia, G. M. Whitesides, *Advanced Materials* **1996,** *8*, 245.

[41] H. C. Clark, L. E. Manzer, *Journal of Organometallic Chemistry* **1973,** *59*, 411.

[42] M. W. Tate, E. F. Eikenberry, S. L. Barna, M. E. Wall, J. L. Lowrance and S. M. Gruner, *J. Appl. Cryst.* **1995**, *28*, 196.